

# Black ringoids: spinning balanced black objects in $d \geq 5$ dimensions – the codimension-two case

---

Burkhard Kleihaus<sup>†</sup>, Jutta Kunz<sup>†</sup> and Eugen Radu<sup>‡</sup>

<sup>†</sup> *Institut für Physik, Universität Oldenburg, Postfach 2503 D-26111 Oldenburg, Germany*

<sup>‡</sup> *Departamento de Física da Universidade de Aveiro and I3N, Campus de Santiago, 3810-183 Aveiro, Portugal*

**ABSTRACT:** We propose a general framework for the study of asymptotically flat black objects with  $k + 1$  equal magnitude angular momenta in  $d \geq 5$  spacetime dimensions (with  $0 \leq k \leq [\frac{d-5}{2}]$ ). In this approach, the dependence on all angular coordinates but one is factorized, which leads to a codimension-two problem. This framework can describe black holes with spherical horizon topology, the simplest solutions corresponding to a class of Myers-Perry black holes. A different set of solutions describes balanced black objects with  $S^{n+1} \times S^{2k+1}$  horizon topology. The simplest members of this family are the black rings ( $k = 0$ ). The solutions with  $k > 0$  are dubbed *black ringoids*. Based on the nonperturbative numerical results found for several values of  $(n, k)$ , we propose a general picture for the properties and the phase diagram of these solutions and the associated black holes with spherical horizon topology:  $n = 1$  black ringoids repeat the  $k = 0$  pattern of black rings and Myers-Perry black holes in 5 dimensions, whereas  $n > 1$  black ringoids follow the pattern of higher dimensional black rings associated with ‘pinched’ black holes and Myers-Perry black holes.

**KEYWORDS:** black holes, numerical solutions.

---

## Contents

<b>1. Introduction</b>	<b>2</b>
<b>2. A special coordinate system</b>	<b>4</b>
2.1 The new coordinates in $D = 4$	5
2.2 The $D > 4$ case and the issue of the metric ansatz	7
<b>3. A general framework</b>	<b>9</b>
3.1 The line element and special cases	9
3.2 The equations	10
3.3 The boundary conditions	12
3.4 Quantities of interest	14
3.4.1 Horizon properties	14
3.4.2 The global charges	15
3.5 Remarks on the numerics	16
<b>4. Exact solutions</b>	<b>17</b>
4.1 A spherical horizon topology: the Myers-Perry black holes	17
4.2 The $d = 5$ Emparan-Reall black ring	22
<b>5. Black objects with non-spherical horizon topology</b>	<b>27</b>
5.1 The blackfold limit	27
5.2 Non-perturbative solutions	27
5.2.1 $k = 0$ : black rings in $d = 6$ dimensions	27
5.2.2 $k = 1$ : black ringoids in $d = 7$ dimensions	33
5.2.3 Further cases and the conjectured picture	39
<b>6. Conclusions and further remarks</b>	<b>40</b>
<b>A. The approximate form of the solutions on the boundaries</b>	<b>42</b>
A.1 The horizon	42
A.2 The $\theta = 0$ boundary	43
A.3 The $\theta = \pi/2$ boundary	44
A.4 The expansion as $r \rightarrow \infty$	45
A.5 On the regularity of the solutions	45
<b>B. Five-dimensional black rings</b>	<b>46</b>
B.1 The solution	46
B.2 The expansion of the metric functions on the boundaries	47

---

## 1. Introduction

The physics of the black hole event horizon has proven a fruitful field of research in gravitational physics. Following Hawking’s black hole topology theorem [1], for many decades the focus was on asymptotically flat black holes in four dimensions with horizons of spherical topology. Also the Tangerlini [2] and the Myers-Perry (MP) [3] black hole solutions, which provide natural higher dimensional generalizations of the  $d = 4$  Schwarzschild and Kerr solutions, respectively, possess horizons of spherical topology. Nevertheless, already Myers and Perry argued that black rings with a horizon topology  $S^2 \times S^1$  should exist [3], making Emparan and Reall’s discovery of the black ring (BR) in  $d = 5$  spacetime dimensions [4, 5] a celebrated and long awaited result.

The discovery of the BRs made clear that a number of well known results in  $d = 4$  gravity do not have a simple extension to higher dimensions. For example, the uniqueness of vacuum black holes is violated in  $d = 5$ , since three distinct solutions may exist for the same global charges (two BRs and a MP black hole). The rapid progress following the discovery in [4, 5] provided a rather extensive picture of the solutions landscape for the five dimensional case, with a large variety of physically interesting solutions (for a review, see [6], [7], [8], [9]).

However, despite the presence of several partial results in the literature, the  $d > 5$  case has remained largely unexplored. At the same time, there is overwhelming evidence that as the dimension increases, the phase structure of the solutions becomes increasingly intricate and diverse, with a variety of other horizon topologies apart from the spherical one [6]. The main obstacle stopping the progress in this field seems to be the absence of closed form solutions (apart from the MP black holes), since the Weyl formalism and various solution generation techniques (which were very useful in  $d = 4, 5$ ) do not apply for the  $d > 5$  asymptotically flat case.

Most of our knowledge in this area is based on results found by using the method of matched asymptotic expansions [10], [11], [12], [13]. Here the central assumption is that some black objects can be approximated by a certain very thin black brane curved into a given shape. In a remarkable development, this has led to the development of the *blackfold effective worldvolume theory*. This theory provides a general formalism leading to quantitative predictions for the behaviour of various  $d > 4$  general relativity solutions in the ultraspinning regime<sup>1</sup>. In this way, it was possible to achieve a partial description of a plethora of higher dimensional black objects with various event horizon topologies.

However, this theory has some clear limitations; for example it is supposed to work only if the length scales involved are widely separated. Also, the blackfold approximation cannot say anything about the issue of the limiting behaviour of the black objects with a nonspherical horizon topology, which is supposed to occur in the region of relatively small angular momenta. Moreover, black holes without a black membrane limiting behavior cannot be described by the blackfold approach [13].

---

<sup>1</sup>This approach is an extension of the theory of classical brane dynamics originally developed by Carter to provide an effective description of some field theory solitons in flat space (see *e.g.* the recent review [14]).

Therefore the construction of higher dimensional black objects with a non-spherical horizon topology within a nonperturbative approach remains a pertinent task. In the absence of exact solutions, this task has been approached recently by employing numerical methods, see *e.g.* the work in [15], [16], [17], [18], [19], [20]. Such an approach can be considered as complementary to the analytical one in [10]-[13]. For example, the numerical results may provide evidence for the existence of the solutions beyond the various approximations employed in the blackfold effective worldvolume theory. At the same time, the analytical predictions there can be used to cross-check the numerical results in some region of the parameter space.

For example, the work [18], [20] has given numerical evidence for the existence of balanced spinning vacuum BRs in  $d > 5$  dimensions and analyzed their basic properties. The results there show that the analytical results from the blackfold approximation work very well for thin BRs. However, a rather complicated picture, which cannot be captured within the blackfold formalism, is found for ‘fat’ BRs. There a different class of solutions starts playing a role – *the ‘pinched’ black holes*. Their existence results from the fact that the ultraspinning MP black holes exhibit a Gregory-Laflamme-type of instability [21, 22]. The ‘pinched’ black holes (which are not yet known in closed form) connect the MP solutions with the branch of ‘fat’ BRs, via a topology changing merger solution [20].

However, apart from the BRs, relatively little is known about the nonperturbative behaviour of other  $d > 5$  solutions with a non-spherical horizon topology. Solutions with an  $S^2 \times S^{d-4}$  horizon topology have been studied in [16], [17]. However, these solutions are static, and supported against collapse by conical singularities.

The main purpose of this paper is to present a general nonperturbative framework capable to describe a class of balanced black object with  $S^{n+1} \times S^{2k+1}$  horizon topology, in  $d \geq 5$  spacetime dimensions,

$$d = 2k + n + 4, \quad \text{with} \quad n \geq 1. \quad (1.1)$$

In this case, the rotation provides a centrifugal repulsion that allows regular solutions to exist. The study here is restricted to the special case of  $k + 1$  equal magnitude angular momenta, with

$$0 \leq k \leq \left[ \frac{d-5}{2} \right], \quad (1.2)$$

an assumption which leads to a treatable codimension-2 numerical problem.

For  $k = 0$ , the framework proposed here reduces to that used in [18] to construct higher dimensional BR solutions. One of the purposes of this work is to present a more detailed discussion of the BRs in [18], together with the properties of the coordinate system introduced there. Apart from that, we shall consider  $d > 6$  solutions with  $k > 0$ , which are dubbed *black ringoids*. Numerical results are reported for the simplest case  $d = 7$ ,  $k = 1$ .

However, apart from these black objects with a non-spherical horizon topology, the proposed framework can describe also a class of MP black holes, whose properties we review

in this work<sup>2</sup>. These MP black holes can also be characterized by the integers  $n$  and  $k$ , associated to the non-rotating and rotating parts of the metric. In particular, they possess  $k + 1$  equal magnitude angular momenta, which is less than the maximally possible number  $N = \lfloor \frac{d-1}{2} \rfloor$  for MP black holes.

When compiling the results for these two different horizon topologies, we are led to conjecture that the basic properties of the  $d > 5$  BRs still hold for  $n > 1$  black ringoids, in particular, for their behaviour in the nonperturbative region, not covered by the blackfold approach. However, we suggest that the solutions with  $n = 1$ , *i.e.* black ringoids with  $S^2 \times S^{d-4}$  horizon topology are special, since they share the basic properties of the  $d = 5$  BRs. This behaviour is related to that of the corresponding MP black holes, which possess an ultraspinning regime for  $n > 1$  only.

This paper is organized as follows: in the next Section we present a discussion of the coordinate system used to impose a non-spherical topology of the event horizon. The general framework is introduced in Section 3. In Section 4 we review the basic properties of the known exact solutions: the  $d \geq 5$  MP black holes with  $k + 1$  equal magnitude angular momenta and the  $d = 5$  Emparan-Reall BRs. We continue with Section 5, where we exhibit the numerical results for several values of  $(d, k)$ . We give our conclusions and remarks in the final Section. The Appendix A contains an approximate form of the solutions on the boundaries of the domain of integration. The expression of the  $d = 5$  balanced BR in the coordinate system introduced in this work is given in Appendix B.

## 2. A special coordinate system

All solutions in this work approach at infinity the Minkowski spacetime background in  $d = D + 1$  dimensions, with a line element

$$ds^2 = -dt^2 + d\sigma_D^2, \quad \text{where} \quad d\sigma_D^2 = d\rho^2 + \rho^2 d\Omega_{d-2}^2, \quad (2.1)$$

and a parametrization of the  $(d - 2)$ -dimensional sphere

$$d\Omega_{d-2}^2 = d\Theta^2 + \cos^2 \Theta d\Omega_n^2 + \sin^2 \Theta d\Omega_p^2, \quad \text{with} \quad D = n + p + 2. \quad (2.2)$$

In the above relations,  $\rho$  and  $t$  are a radial and a time coordinate, respectively, while  $\Theta$  is an angular coordinate, with  $0 \leq \Theta \leq \pi/2$ . Also,  $d\Omega_n^2$  is the metric on the  $n$ -dimensional sphere. For  $d = 5$ , these are the usual bi-azimuthal coordinates, with  $n = p = 1$  and

$$d\sigma_4^2 = d\rho^2 + \rho^2(d\Theta^2 + \cos^2 \Theta d\phi^2 + \sin^2 \Theta d\psi^2), \quad \text{with} \quad 0 \leq (\phi, \psi) < 2\pi. \quad (2.3)$$

The numerical scheme used in this work requires a rectangular boundary for the coordinates, such that both the event horizon and the spacelike infinity are located at a constant

---

<sup>2</sup>Moreover, the ‘pinched’ black holes (which also possess a horizon of spherical topology) can be studied as well within the proposed framework, although we do not consider them here.

value of one of the coordinates. As we shall see in Section 4, this is possible for MP black holes, where a surface of constant radial coordinate in a general line element based on (2.1) is topologically a sphere.

In what follows, we show the existence of a parametrization of the flat space with the property that (2.1) is approached only asymptotically, while a surface of constant (new) radial coordinate possesses, for some of its range, a  $S^{n+1} \times S^p$  topology<sup>3</sup>.

## 2.1 The new coordinates in $D = 4$

The coordinates usually used in the study of  $d = 5$  BRs naturally occur when considering a foliation of the  $D = 4$  flat space in terms of the equipotential surfaces of a two form potential sourced by a ring [25]. In these coordinates, the flat space metric reads

$$ds^2 = \frac{R^2}{(x-y)^2} \left[ \frac{dx^2}{1-x^2} + \frac{dy^2}{y^2-1} + (1-x^2)d\phi^2 + (y^2-1)d\psi^2 \right], \quad (2.4)$$

with  $R > 0$  an arbitrary parameter and

$$-\infty < y < -1, \quad -1 \leq x \leq 1. \quad (2.5)$$

Although these coordinates are physically rather opaque, they result in a simple and compact form of the  $d = 5$  BR solution. However, in a numerical approach, their disadvantage is that the asymptotic infinity is approached at a single point,  $x \rightarrow -1$ ,  $y \rightarrow -1$ . Therefore, the imposition of the boundary conditions and the extraction of the mass and the angular momenta of the solutions is problematic, at least for the scheme used in this work, and represents an obstacle which we could not overcome so far.

We solve this problem by working with a different coordinate system, with a foliation of the flat space in terms of equipotential surfaces of a scalar field  $\Psi$  solving the Laplace equation

$$\nabla^2 \Psi = 0, \quad (2.6)$$

outside of a ring source at  $\rho = R > 0$ ,  $\Theta = 0$ . The corresponding solution reads

$$\Psi(\rho, \Theta) = \frac{1}{\sqrt{(R^2 + \rho^2)^2 - 4R^2 \rho^2 \cos^2 \Theta}}. \quad (2.7)$$

---

<sup>3</sup>It is interesting to notice the formal analogy with the Kaluza-Klein caged black holes in  $d$ -dimensions. In some sense, those solutions are the opposite of the BRs, possessing a spherical horizon topology, and approaching, however, a background which is the product of the Minkowski spacetime with a circle. The numerical problem of constructing solutions with this behaviour has been solved in [23] by using a special coordinate system in the spirit of the one introduced in Section (2.1) (see also [24]). For the coordinate system in [23], a surface of constant radial coordinate has the topology  $S^{d-2}$  close to the horizon and  $S^{d-3} \times S^1$  in the asymptotic region.

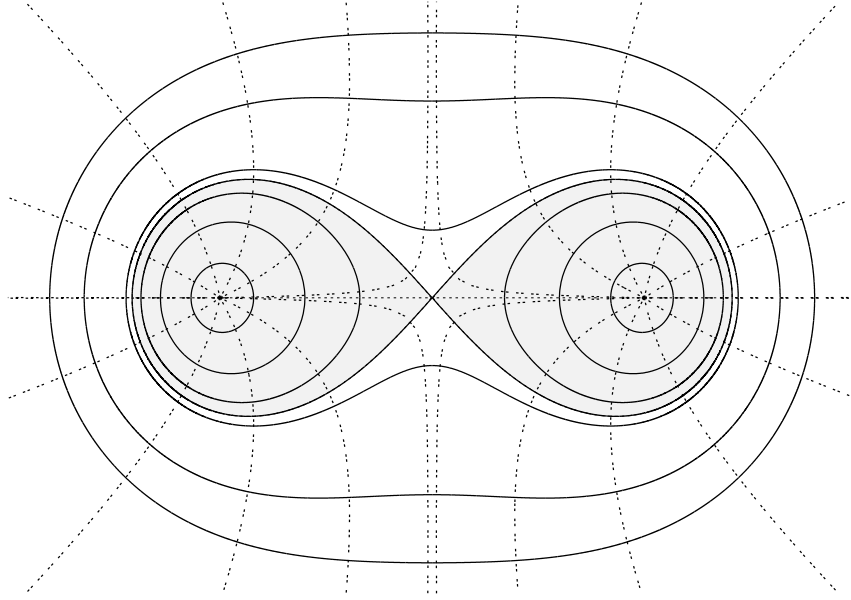


**Figure 1.** The new coordinates for the  $D = 4$  flat space metric on a section at constant  $\phi$  and  $\psi$  (and  $\phi + \pi$  and  $\psi + \pi$ ). The solid lines shown here have constant values of  $r$ , while the dotted lines have constant  $\theta$ . Also, the shaded gray region covers the domain  $r < R$ .

Then, following the corresponding approach in [25] for a two form potential, we introduce the new coordinates  $(r, \theta)$  that correspond to surfaces of constant  $\Psi$  and their gradients surfaces.

The coordinate transformation between  $(\rho, \Theta)$  in (2.3) and  $(r, \theta)$  is

$$\rho = r\sqrt{U(r, \theta)}, \quad \tan \Theta = \left(\frac{r^2 + \rho^2 + R^2}{r^2 + \rho^2 - R^2}\right) \tan \theta, \quad (2.8)$$

the relation with the usual ring coordinates  $(x, y)$  being

$$x = \frac{R^2}{r^2} - U(r, \theta), \quad y = -\frac{R^2}{r^2} - U(r, \theta). \quad (2.9)$$

In the above relations we note

$$U(r, \theta) = \sqrt{1 + \frac{R^4}{r^4} - \frac{2R^2}{r^2} \cos 2\theta}. \quad (2.10)$$

The coordinate range here is  $0 \leq r < \infty$ ,  $0 \leq \theta \leq \pi/2$ .

A straightforward computation leads to the following expression of the  $D = 4$  flat space line element as written in  $(r, \theta)$ -coordinates

$$d\sigma_4^2 = F_1(r, \theta)(dr^2 + r^2 d\theta^2) + F_2(r, \theta)d\psi^2 + F_3(r, \theta)d\phi^2, \quad (2.11)$$

where

$$F_1(r, \theta) = \frac{1}{U}, \quad F_2(r, \theta) = r^2 \left( \cos^2 \theta - \frac{1}{2} \left( 1 + \frac{R^2}{r^2} - U \right) \right), \quad F_3(r, \theta) = r^2 \left( \sin^2 \theta - \frac{1}{2} \left( 1 - \frac{R^2}{r^2} - U \right) \right), \quad (2.12)$$

with  $U$  given by (2.10).

Since  $r$  runs from zero to infinity, one can think of it as a sort of radial coordinate. As  $r \rightarrow 0$ , the behaviour of the metric functions is

$$F_1 = \frac{r^2}{R^2} + O(r^4), \quad F_2 = \frac{r^4}{R^2} \sin^2 \theta \cos^2 \theta + O(r^6), \quad F_3 = R^2 + O(r^2). \quad (2.13)$$

By defining  $r = \sqrt{2R\bar{r}}$ ,  $\theta = \bar{\theta}/2$ , one can show that  $r = 0$  is a regular origin, with

$$ds^2 = d\bar{r}^2 + \bar{r}^2 d\bar{\theta}^2 + \bar{r}^2 \sin^2 \bar{\theta} d\psi^2 + R^2 d\phi^2, \quad (2.14)$$

in the vicinity of that point.

In fact, one can see that for  $0 < r < R$ , a surface of constant  $r$  has a  $S^2 \times S^1$  topology, where the  $S^2$  is parametrized by  $(\theta, \psi)$  and the  $S^1$  by  $\phi$ . For  $r > R$ , one recovers the usual  $S^3$  topology of an  $r = \text{const.}$  foliation.  $r = R$ ,  $\theta = 0$  is a special point with a coordinate system singularity. These features are shown in Fig. 1, where we present a section at constant  $\phi$  and  $\psi$ . (Note that, for greater clarity, the antipodal sections at  $\phi + \pi$  and  $\psi + \pi$  are also shown there.)

It is also useful to consider the expansion of the functions  $F_i$  at  $\theta = 0, \pi/2$ . Starting with  $\theta = 0$ , one finds

$$F_1 = \frac{r^2}{R^2 - r^2} + O(\theta^2), \quad F_2 = \frac{r^4}{R^2 - r^2} \theta^2 + O(\theta^4), \quad F_3 = R^2 - r^2 + O(\theta^2),$$

for  $r < R$ , and

$$F_1 = \frac{r^2}{r^2 - R^2} + O(\theta^2), \quad F_2 = r^2 - R^2 + O(\theta^2), \quad F_3 = \frac{r^4}{R^2 - r^2} \theta^2 + O(\theta^4),$$

for  $r > R$ . The corresponding expansion for  $\theta = \pi/2$  is

$$F_1 = \frac{r^2}{r^2 + R^2} + O(\theta - \frac{\pi}{2})^2, \quad F_2 = \frac{r^4}{r^2 + R^2} (\theta - \frac{\pi}{2})^2 + O(\theta^4), \quad F_3 = (r^2 + R^2) + O(\theta - \frac{\pi}{2})^2.$$

For completeness, we give also the asymptotic form of the functions valid for large  $r$

$$F_1 = 1 + \frac{R^2}{r^2} \cos 2\theta + O(1/r^4), \quad F_2 = r^2 \cos^2 \theta (1 - \frac{R^2}{r^2}) + O(1/r^2), \quad F_3 = r^2 \sin^2 \theta (1 + \frac{R^2}{r^2}) + O(1/r^2),$$

such that asymptotically  $(r, \theta)$  correspond to the usual bi-azimuthal coordinates.

## 2.2 The $D > 4$ case and the issue of the metric ansatz

The above coordinates generalize straightforwardly to  $D > 4$  dimensions<sup>4</sup>. By using the same transformation (2.8), the flat space line element  $d\sigma_D^2$  in (2.1), (2.2) becomes

$$ds^2 = F_1(r, \theta)(dr^2 + r^2 d\theta^2) + F_2(r, \theta) d\Omega_n^2 + F_3(r, \theta) d\Omega_p^2, \quad (2.15)$$

---

<sup>4</sup>Note that the interpretation of the  $(r, \theta)$  coordinates as corresponding to equipotential surfaces of a scalar field is lost for  $D > 4$ . Although one can devise such a coordinate system, the resulting expressions are too complicated to use in practice.



with the same expression (2.12) for the  $F_i$  and the same coordinate range for  $(r, \theta)$ . Then, for  $0 < r < R$ , a surface of constant  $r$  has a  $S^{n+1} \times S^p$  topology, while for  $r > R$ , an  $r = \text{const.}$  surface is topologically a sphere.

It is now obvious that this parametrization of flat space can be used to describe black objects with a non-spherical horizon topology. The corresponding line element in  $d = D + 1$  dimensions should preserve the basic structure of (2.15) (*e.g.* the behaviour at  $\theta = 0, \pi/2$ ), containing, however, additional terms that encode the gravity effects. The event horizon will be located at a constant (positive) value of  $r < R$ , and so the black objects will inherit the  $S^{n+1} \times S^p$  topology. For values larger than  $R$ , the coordinate  $r$  would correspond to the usual radial coordinate.

However, the metric ansatz should also be general enough to allow for rotation<sup>5</sup>. Then the centrifugal force would prevent the collapse of such black objects with a non-spherical horizon topology, and balance them. A generic metric ansatz based on (2.15) which describes a rotating spacetime, would contain metric functions with a nontrivial dependence of at least one more coordinate apart from  $r, \theta$ . However, this is a very hard numerical problem which we have not yet solved.

However, the problem is greatly simplified for the special case

$$p = 2k + 1, \quad \text{with } k \geq 0, \quad (2.16)$$

by assuming that all angular momenta on the  $S^p$  have equal magnitude. At the same time, all other possible angular momenta vanish. (We recall that in  $d$  spacetime dimensions, there are  $N = \lfloor \frac{d-1}{2} \rfloor$  independent angular momenta.) This would factorize the dependence of the coordinates on  $S^p$ , leading to a cohomogeneity-2 ansatz, the resulting equations of motion forming a set of coupled nonlinear PDEs in terms of  $(r, \theta)$  only.

The inclusion of rotation on the  $S^{2k+1}$  is based on the simple observation that one can always write the metric of an odd-dimensional (round) sphere as an  $S^1$  fibration over the complex projective space  $\mathbb{CP}^k$ ,

$$d\Omega_{2k+1}^2 = (d\psi + \mathcal{A})^2 + d\Sigma_k^2, \quad (2.17)$$

where  $d\Sigma_k^2$  is the metric on the unit  $\mathbb{CP}^k$  space and  $\mathcal{A} = A_i dx^i$  is its Kähler form. The fibre is parameterized by the coordinate  $\psi$ , which has period  $2\pi$ .

A simple explicit form for (2.17) is found by introducing  $k + 1$  complex coordinates  $z_i$

---

<sup>5</sup>Unfortunately, the only way to achieve balance for a non-spherical horizon topology seems to be to rotate the solutions. To our knowledge, no other mechanism is known at this moment. For example, the results in [26] show that the Gauss-Bonnet corrections to Einstein gravity cannot eliminate the conical singularity of a  $d = 5$  static BR. A similar result is likely to hold also for the Einstein-Gauss-Bonnet generalizations of the higher dimensional configurations discussed in this work.

(with  $\sum_i^{k+1} z_i \bar{z}_i = 1$ ), such that  $d\Omega_{2k+1}^2 = \sum_i dz_i d\bar{z}_i$ . A simple expression of  $z_i$  is (see *e.g.* [27]):

$$z_i = e^{i(\psi + \phi_i)} \cos \theta_i \prod_{j < i} \sin \theta_j, \quad \text{for } i = 1, \dots, k, \quad \text{and} \quad z_{k+1} = e^{i\psi} \prod_{j=1}^{\frac{n-1}{2}} \sin \theta_j. \quad (2.18)$$

(Note that the coordinates  $\phi_i$  have period  $2\pi$  while the  $\theta_i$  have period  $\pi/2$ .) The corresponding expression of the Kähler form  $\mathcal{A}$  is

$$\mathcal{A} = A_i dx^i = \sum_{i=1}^k \cos^2 \theta_i \left[ \prod_{j < i} \sin^2 \theta_j \right] d\phi_i. \quad (2.19)$$

In this approach<sup>6</sup>, the rotation will be introduced by adding an extra term  $Wdt$  to the form  $d\psi + \mathcal{A}$ . Also, the rotation will deform the sphere  $S^{2k+1}$ , with different factors for the two parts in (2.17).

### 3. A general framework

#### 3.1 The line element and special cases

The above considerations lead to the following metric ansatz:

$$ds^2 = f_1(r, \theta) (dr^2 + \Delta(r) d\theta^2) + f_2(r, \theta) d\Omega_n^2 - f_0(r, \theta) dt^2 \\ + f_3(r, \theta) (d\psi + \mathcal{A} - W(r, \theta) dt)^2 + f_4(r, \theta) d\Sigma_k^2, \quad (3.1)$$

which can be used to describe a class of black objects with a  $S^{n+1} \times S^{2k+1}$  horizon topology. However, as we shall see in the next Section, the MP black holes with  $k+1$  equal angular momenta can also be written in the above form.

In our approach, the information on the solutions is encoded in the unknown functions  $(f_i, W)$ , ( $i = 0, \dots, 4$ ). Note that the dependence of the coordinates on the  $S^{2k+1}$  factorizes, such that the problem is effectively codimension-2. Also,  $\Delta(r)$  is a given ‘background’ function which is chosen for convenience by using the residual metric gauge freedom. In the numerical study of the solutions with non-spherical horizon topology, we set

$$\Delta(r) = r^2, \quad (3.2)$$

without any loss of generality. However, as we shall see, the MP black holes take a simple form for a different choice of  $\Delta(r)$ .

---

<sup>6</sup>Note that a similar approach has been used in the literature to numerically construct  $d \geq 5$  spinning black holes with a spherical horizon topology, for various theories where an exact solution is missing, see *e.g.* [28], [29], [30], [27] (as well as in the perturbative construction of exact solutions [31],[32]). Note that in all these cases it was possible to reduce the problem to solving a set of ordinary differential equations. However, a non-spherical horizon topology prevents this possibility.

	<i>spherical horizon</i>	<i>black rings</i>	<i>black ringoids</i>		
	MP/‘pinched’	$k = 0$	$k = 1$	$k = 2$	$k = 3$
$d = 5$	$S^3$	$\mathbf{S}^2 \times \mathbf{S}^1$			
$d = 6$	$S^4$	$S^3 \times S^1$			
$d = 7$	$S^5$	$S^4 \times S^1$	$\mathbf{S}^2 \times \mathbf{S}^3$		
$d = 8$	$S^6$	$S^5 \times S^1$	$S^3 \times S^3$		
$d = 9$	$S^7$	$S^6 \times S^1$	$S^4 \times S^3$	$\mathbf{S}^2 \times \mathbf{S}^5$	
$d = 10$	$S^8$	$S^7 \times S^1$	$S^5 \times S^3$	$S^3 \times S^5$	
$d = 11$	$S^9$	$S^8 \times S^1$	$S^6 \times S^3$	$S^4 \times S^5$	$\mathbf{S}^2 \times \mathbf{S}^7$

**Table 1.** A list of horizon topologies for spinning balanced black objects which can be described by the metric ansatz (3.1).

The range of the radial coordinate is  $r_H \leq r < \infty$ , and  $r = r_H > 0$  corresponds to the event horizon, where  $f_0(r_H, \theta) = 0$ . Also, the angular coordinate  $\theta$  has the usual range,  $0 \leq \theta \leq \pi/2$ . Thus the domain of integration has a rectangular shape, and is well suited for numerical calculations.

The case  $k = 0$  is special, since the  $d\Sigma_k^2$  term is absent in this case (also  $\mathcal{A} = 0$ ), with a line element

$$ds^2 = f_1(r, \theta) (dr^2 + \Delta(r)d\theta^2) + f_2(r, \theta)d\Omega_{d-3}^2 + f_3(r, \theta)(d\psi - W(r, \theta)dt)^2 - f_0(r, \theta)dt^2, \quad (3.3)$$

describing black objects with  $S^{d-3} \times S^1$  topology of the event horizon (*i.e.* the BRs), as well as MP black holes rotating in a single plane. (Note that the ‘pinched’ black holes in [20] can also be studied within this ansatz.) The corresponding relations are found by taking formally  $k = 0$ ,  $f_4 = 1$  in all general equations exhibited below.

Another case of interest is  $n = 1$ , with a line element

$$ds^2 = f_1(r, \theta) (dr^2 + \Delta(r)d\theta^2) + f_2(r, \theta)d\phi^2 - f_0(r, \theta)dt^2 + f_3(r, \theta)(d\psi + \mathcal{A} - W(r, \theta)dt)^2 + f_4(r, \theta)d\Sigma_k^2, \quad (3.4)$$

describing black objects with a  $S^2 \times S^{d-4}$  topology of the event horizon in  $d = 2k + 5$  dimensions. (Therefore, the  $d = 5$  line-element (3.3) is the first member of this family.) As we shall see, the properties of the solutions are special in this case<sup>7</sup>.

Finally, in Table 1 we give a list of possible horizon topologies which can be studied within this framework, for  $5 \leq d \leq 11$  (the special case  $n = 1$  is highlighted there).

### 3.2 The equations

A suitable combination of the Einstein equations  $G_r^r + G_\theta^\theta = 0$ ,  $G_\Omega^\Omega = 0$ ,  $G_\psi^\psi = 0$ ,  $G_\Sigma^\Sigma = 0$ ,  $G_\psi^t = 0$ ,  $G_t^t = 0$  (with  $G_\mu^\nu$  the Einstein tensor), yield for the functions  $(f_i, W)$  the following

---

<sup>7</sup>The static limit of (3.4) has  $f_3 = f_4$ ,  $W = 0$ , and exists for any  $d \geq 5$ . The properties of the static un-balanced black objects with  $S^2 \times S^{d-4}$  topology of the event horizon are discussed in [16].

set of equations:

$$\begin{aligned} \nabla^2 f_0 - \frac{1}{2f_0}(\nabla f_0)^2 + \frac{(d-2k-4)}{2f_2}(\nabla f_0) \cdot (\nabla f_2) + \frac{1}{2f_3}(\nabla f_0) \cdot (\nabla f_3) \\ - f_3(\nabla W)^2 + \frac{k}{f_4}(\nabla f_0) \cdot (\nabla f_4) = 0. \end{aligned} \quad (3.5)$$

$$\begin{aligned} \nabla^2 f_1 - \frac{1}{f_1}(\nabla f_1)^2 - \frac{(d-2k-4)f_1}{2f_0f_2}(\nabla f_0) \cdot (\nabla f_2) - \frac{(d-2k-4)(d-2k-5)f_1}{4f_2^2}(\nabla f_2)^2 \\ - \frac{f_1}{2f_0f_3}(\nabla f_0) \cdot (\nabla f_3) - \frac{(d-2k-4)f_1}{2f_2f_3}(\nabla f_2) \cdot (\nabla f_3) - \frac{f_1f_3}{2f_0}(\nabla W)^2 - f_1 \left( \frac{\Delta'^2}{2\Delta^2} - \frac{\Delta''}{\Delta} \right) \\ + \frac{(d-2k-4)(d-2k-5)f_1^2}{f_2} + k \left( -\frac{f_1}{f_0f_4}(\nabla f_0) \cdot (\nabla f_4) - \frac{(d-2k-4)f_1}{f_2f_4}(\nabla f_2) \cdot (\nabla f_4) \right. \\ \left. - \frac{f_1}{f_3f_4}(\nabla f_3) \cdot (\nabla f_4) - \frac{(2k-1)f_1}{2f_2^2}(\nabla f_4)^2 + \frac{2f_1^2}{f_4}(2(k+1) - \frac{f_3}{f_4}) \right) = 0, \end{aligned} \quad (3.6)$$

$$\begin{aligned} \nabla^2 f_2 + \frac{1}{2f_0}(\nabla f_2) \cdot (\nabla f_0) + (d-2k-6)\frac{1}{2f_2}(\nabla f_2)^2 + \frac{1}{2f_3}(\nabla f_2) \cdot (\nabla f_3) \\ + \frac{k}{f_4}(\nabla f_2) \cdot (\nabla f_4) - 2(d-2k-5)f_1 = 0, \end{aligned} \quad (3.7)$$

$$\begin{aligned} \nabla^2 f_3 + \frac{1}{2f_0}(\nabla f_3) \cdot (\nabla f_0) + (d-2k-4)\frac{1}{2f_2}(\nabla f_2) \cdot (\nabla f_3) - \frac{1}{2f_3}(\nabla f_3)^2 \\ + \frac{f_3^2}{f_0}(\nabla W)^2 - \frac{4kf_1f_3^2}{f_4^2} + k\frac{1}{f_4}(\nabla f_3) \cdot (\nabla f_4) = 0, \end{aligned} \quad (3.8)$$

$$\begin{aligned} \nabla^2 f_4 + \frac{1}{2f_0}(\nabla f_4) \cdot (\nabla f_0) + (d-2k-4)\frac{1}{2f_2}(\nabla f_2) \cdot (\nabla f_4) + \frac{1}{2f_3}(\nabla f_3) \cdot (\nabla f_4) \\ + \frac{(k-1)}{f_4}(\nabla f_4)^2 - 4(k+1)f_1 + \frac{4f_1f_3}{f_4} = 0, \end{aligned} \quad (3.9)$$

$$\begin{aligned} \nabla^2 W - \frac{1}{2f_0}(\nabla W) \cdot (\nabla f_0) + (d-2k-4)\frac{1}{2f_2}(\nabla W) \cdot (\nabla f_2) \\ + \frac{3}{2f_3}(\nabla W) \cdot (\nabla f_3) + \frac{k}{f_4}(\nabla W) \cdot (\nabla f_4) = 0. \end{aligned} \quad (3.10)$$

All other Einstein equations except for  $G_r^\theta = 0$  and  $G_r^r - G_\theta^\theta = 0$  are linear combinations of those used to derive the above equations or are identically zero. The remaining equations

$G_r^\theta = 0$  and  $G_r^r - G_\theta^\theta = 0$  yield two constraints

$$\begin{aligned}
& -\frac{\Delta'}{4\Delta} \left( (d-2k-4) \frac{f_2'}{f_2} + \frac{f_3'}{f_3} + \frac{f_0'}{f_0} \right) - \frac{1}{4f_0^2} (f_0'^2 - \frac{1}{\Delta} \dot{f}_0^2) - \frac{1}{2f_0 f_1} (f_0' f_1' - \frac{1}{\Delta} \dot{f}_0 \dot{f}_1) \\
& - \frac{(d-2k-4)}{2f_1 f_2} (f_1' f_2' - \frac{1}{\Delta} \dot{f}_1 \dot{f}_2) - \frac{(d-2k-4)}{4f_2^2} (f_2'^2 - \frac{1}{\Delta} \dot{f}_2^2) - \frac{1}{2f_1 f_3} (f_1' f_3' - \frac{1}{\Delta} \dot{f}_1 \dot{f}_3) \\
& - \frac{f_3}{2f_0} (W'^2 - \frac{1}{\Delta} \dot{W}^2) - \frac{1}{4f_3^2} (f_3'^2 - \frac{1}{\Delta} \dot{f}_3^2) + \frac{1}{2f_0} (f_0'' - \frac{1}{\Delta} \ddot{f}_0) + \frac{(d-2k-4)}{2f_2} (f_2'' - \frac{1}{\Delta} \ddot{f}_2) \\
& + \frac{1}{2f_3} (f_3'' - \frac{1}{\Delta} \ddot{f}_3) + k \left( f_4'' - \frac{1}{\Delta} \ddot{f}_4 - \frac{\Delta'}{\Delta} \frac{f_4'}{2f_4} - \frac{1}{f_1 f_4} (f_1' f_4' - \frac{1}{\Delta} \dot{f}_1 \dot{f}_4) - \frac{1}{2f_4^2} (f_4'^2 - \frac{1}{\Delta} \dot{f}_4^2) \right) = 0,
\end{aligned} \tag{3.11}$$

$$\begin{aligned}
& -\frac{\Delta'}{4\Delta} \left( \frac{\dot{f}_0}{f_0} + \frac{(d-2k-4)\dot{f}_2}{f_2} + \frac{\dot{f}_3}{f_3} \right) - \frac{1}{4f_0 f_1} (\dot{f}_1 f_0' + \dot{f}_0 f_1') - \frac{(d-2k-4)}{4f_1 f_2} (\dot{f}_2 f_1' + \dot{f}_1 f_2') \\
& - \frac{1}{4f_1 f_3} (\dot{f}_1 f_3' + \dot{f}_3 f_1') - \frac{1}{4f_0^2} \dot{f}_0 f_0' - \frac{(d-2k-4)}{4f_2^2} \dot{f}_2 f_2' - \frac{1}{4f_3^2} \dot{f}_3 f_3' - \frac{f_3}{2f_0} \dot{W} W' \\
& + \frac{1}{2} \left( \frac{\dot{f}_0'}{f_0} + \frac{(d-2k-4)\dot{f}_2'}{f_2} + \frac{\dot{f}_3'}{f_3} \right) + k \left( \frac{\dot{f}_4'}{f_4} - \frac{\dot{f}_4 f_4'}{2f_4^2} - \frac{1}{2f_1 f_4} (\dot{f}_1 f_4' + \dot{f}_4 f_1' - \frac{\Delta'}{\Delta} \frac{\dot{f}_4}{2f_4}) \right) = 0.
\end{aligned} \tag{3.12}$$

In the above relations, a prime denotes  $\partial/\partial_r$ , and a dot  $\partial/\partial_\theta$ . Also, we have defined

$$\begin{aligned}
(\nabla A) \cdot (\nabla B) &= A' B' + \frac{1}{\Delta} \dot{A} \dot{B}, \\
\nabla^2 A &= A'' + \frac{1}{\Delta} \ddot{A}.
\end{aligned}$$

One can easily verify that the Minkowski spacetime background is recovered for

$$f_1 = F_1, \quad f_2 = F_2, \quad f_3 = f_4 = F_3, \quad f_0 = 1, \quad W = 0, \tag{3.13}$$

with  $F_i, \Delta$  given by (2.12) and (3.2), respectively.

The structure of these equations suggests that the case  $n = 1$ , *i.e.*  $d = 2k + 5$ , is special, since some source terms associated with the curvature of the  $S^n$ -part of the metric vanish in this case. As we shall see, the properties of the corresponding solutions with  $S^2 \times S^{d-4}$  horizon topology are indeed different, as well as those of the corresponding MP black holes.

### 3.3 The boundary conditions

In Appendix A we give an approximate form of the solutions on the boundaries of the domain of integration, compatible with the  $S^{n+1} \times S^{2k+1}$  and  $S^{d-2}$  horizon topologies. The analysis there leads to a natural set of boundary conditions for the solutions in this work, which are imposed in the numerics. First, the boundary conditions satisfied at the horizon,  $r = r_H$ , are

$$f_0 = 0, \quad r_H \partial_r f_1 + 2f_1 = \partial_r f_2 = \partial_r f_3 = 0, \quad W = \Omega_H. \tag{3.14}$$

As  $r \rightarrow \infty$ , the Minkowski spacetime background is recovered, which implies

$$f_0 = f_1 = 1, \quad f_2 = r^2 \cos^2 \theta, \quad f_3 = f_4 = r^2 \sin^2 \theta, \quad W = 0. \tag{3.15}$$

At  $\theta = \pi/2$ , we impose

$$\partial_\theta f_0 = \partial_\theta f_1 = f_2 = \partial_\theta f_3 = \partial_\theta f_4 = \partial_\theta W = 0. \quad (3.16)$$

The boundary conditions at  $\theta = 0$  are more complicated. For solutions with a  $S^{n+1} \times S^{2k+1}$  horizon topology, we impose

$$\partial_\theta f_0 = \partial_\theta f_1 = f_2 = \partial_\theta f_3 = \partial_\theta f_4 = \partial_\theta W = 0, \quad (3.17)$$

for  $r_H < r \leq R$ , and

$$\partial_\theta f_0 = \partial_\theta f_1 = \partial_\theta f_2 = f_3 = f_4 = \partial_\theta W = 0, \quad (3.18)$$

for  $r_H > R$ . The solutions with a spherical horizon topology are subject to the conditions (3.18) for any  $r > r_H$ . (We recall that  $R$  does not appear in this case.)

Apart from that, the solutions on the boundaries are subject to a number of extra-conditions, originating mainly in the constraint equations (*e.g.* the constancy of the Hawking temperature on the horizon, see the analysis in Appendix A). However, these conditions are not imposed in the numerics, but used to verify the accuracy of the results.

In describing the boundary conditions (3.14)-(3.17), we have found it useful<sup>8</sup> to introduce the diagrams shown in Figure 2. There, the domain of integration is shown together with the boundary conditions satisfied by some metric functions which enter the angular part of the metric (with  $g_{\Omega\Omega} = f_2$  and  $g_{\Sigma\Sigma} = f_3, f_4$ ). In our conventions, a wavy line indicates a horizon, a dotted line represents infinity, a thick line means that the coefficient  $g_{\Omega\Omega}$  vanishes and a double thin line stands for  $g_{\Sigma\Sigma} = 0$ . Thus, the horizon topology can easily be read from such diagrams: a spherical horizon continues with thick and double thin lines, while for a  $S^{n+1} \times S^{2k+1}$  horizon topology, the horizon continues with thick lines only (*i.e.* the coefficient of the  $d\Omega_n^2$  part of the metric vanishes both at  $\theta = 0$  and  $\theta = \pi/2$ ).

Finally, let us mention that the diagrams in Figure 2 encode also the generalized rod-structure of the solutions; moreover, for  $d = 5$  they help to make contact with the usual Weyl coordinates. A discussion of these aspects can be found in [17]. As shown there, similar diagrams can be drawn to describe composite black objects, *e.g.* black Saturns or dirings.

---

<sup>8</sup>These diagrams should also be viewed together with the plots of the metric functions in the Figures 3, 4, 8, 12.

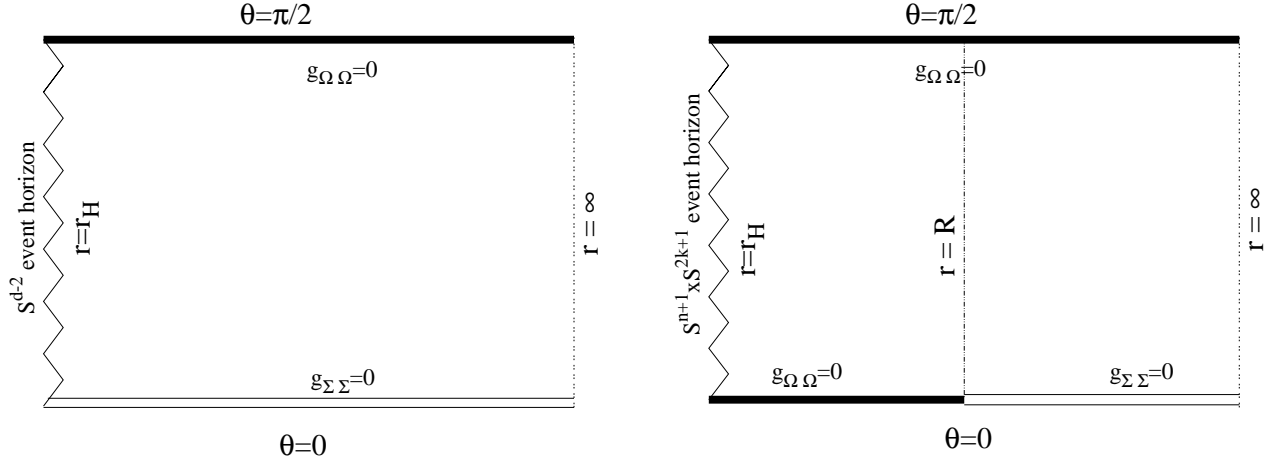


**Figure 2.** The domain of integration for the solutions in this work is shown for a black hole with spherical horizon topology and a black object with  $S^{n+1} \times S^{2k+1}$  horizon topology.

### 3.4 Quantities of interest

#### 3.4.1 Horizon properties

As discussed above, for any topology, the horizon is located at a constant value of the radial coordinate,  $r = r_H$ . The metric of a spatial cross-section of the horizon is

$$d\sigma^2 = f_1(r_H, \theta) r_H^2 d\theta^2 + f_2(r_H, \theta) d\Omega_n^2 + f_3(r_H, \theta) (d\psi + \mathcal{A})^2 + f_4(r_H, \theta) d\Sigma_k^2. \quad (3.19)$$

From the above boundary conditions and the discussion in Section 3.3, it is clear that the topology of the horizon of the generic solutions is  $S^{n+1} \times S^{2k+1}$  (although both  $S^{n+1}$  and  $S^{2k+1}$  are not round spheres). The crucial point here is that the functions  $f_3, f_4$  multiplying the  $S^{2k+1}$  part are nonzero for any  $r \leq R$ , while  $f_2$  vanishes as  $\epsilon^2$  at both  $\theta = 0$  and  $\theta = \pi/2$  (which will correspond to the poles of the  $S^{n+1}$ -sphere).

However, the same horizon metric is shared by black objects with an  $S^{d-2}$  horizon topology, in which case  $f_2$  vanishes at  $\theta = \pi/2$  (with  $f_3, f_4$  nonzero), while  $f_3, f_4$  are zero at  $\theta = 0$  (with  $f_2$  nonvanishing there).

For any horizon topology, the event horizon area  $A_H$ , Hawking temperature  $T_H$  and event horizon velocity  $\Omega_H$  of the solutions are given by

$$A_H = r_H V_{(n)} V_{(2k+1)} \int_0^{\pi/2} d\theta \sqrt{f_1 f_2^n f_3 f_4^{2k}} \Big|_{r=r_H}, \quad (3.20)$$

$$T_H = \frac{1}{2\pi} \lim_{r \rightarrow r_H} \frac{1}{(r - r_H)} \sqrt{\frac{f_0}{f_1}}, \quad \Omega_H = W|_{r=r_H},$$

where  $V_{(p)}$  is the area of the unit  $S^p$  sphere. Also, one can see that the Killing vector

$$\xi = \partial/\partial_t + \Omega_H \partial/\partial_\psi \quad (3.21)$$

is orthogonal and null on the horizon.

For black holes with a non-spherical horizon topology, it is useful to get some estimates for the deformation of the two parts in the horizon metric (3.19). To obtain a measure for the deformation of the  $S^{d-3}$  sphere, we compare the circumference at the equator,  $L_e$  ( $\theta = \pi/4$ , where the sphere is fattest), with the circumference of the  $S^{n+1}$  along the poles,  $L_p$ ,

$$L_e = 2\pi\sqrt{f_2(r_H, \pi/4)}, \quad L_p = 2 \int_0^{\pi/2} d\theta \, r_H \sqrt{f_1(r_H, \theta)}, \quad (3.22)$$

and consider, in particular, their ratio  $L_e/L_p$ . The sphere  $S^{2k+1}$  in (3.19) is also deformed; a possible estimate of its deformation is given by the ratio  $R_{2k+1}^{(in)}/R_{2k+1}^{(out)}$ , where we define

$$R_{2k+1}^{(in)} = \left( f_3(r_H, 0) f_4^{2k}(r_H, 0) \right)^{\frac{1}{2(2k+1)}}, \quad R_{2k+1}^{(out)} = \left( f_3(r_H, \pi/2) f_4^{2k}(r_H, \pi/2) \right)^{\frac{1}{2(2k+1)}}. \quad (3.23)$$

These expressions are found by introducing an effective ( $\theta$ -dependent) radius of the  $S^{2k+1}$  via its area, and taking its value inside the ring(oid) at  $\theta = 0$ , and outside at  $\theta = \pi/2$ .

### 3.4.2 The global charges

The mass and angular momenta are read from the large- $r$  asymptotics of the metric functions,  $g_{tt} = -1 + \frac{C_t}{r^{d-3}} + \dots$ ,  $g_{\psi t} = -f_3 W = \frac{C_\psi}{r^{d-3}} \sin^2 \theta + \dots$ , with ( $G = 1$ ):

$$\mathcal{M} = \frac{(d-2)V_{(d-2)}}{16\pi} C_t, \quad J_1 = \dots = J_{k+1} = J, \quad \text{where} \quad J = \frac{V_{(d-2)}}{8\pi} C_\psi. \quad (3.24)$$

Also, the solutions satisfy the Smarr relation

$$\frac{d-3}{d-2} \mathcal{M} = T_H \frac{A_H}{4} + (k+1) \Omega_H J, \quad (3.25)$$

and the 1<sup>st</sup> law

$$d\mathcal{M} = \frac{1}{4} T_H dA_H + (k+1) \Omega_H dJ. \quad (3.26)$$

The black objects have an entropy which is given by the area law,  $S = \frac{A_H}{4}$ .

It is well-known that different thermodynamic ensembles are not exactly equivalent (for example they may not lead to the same conclusions regarding the thermodynamic stability as they correspond to different physical situations). We study the solutions in a canonical ensemble by keeping the temperature  $T_H$  and the angular momentum fixed. The associated thermodynamic potential is the Helmholtz free energy

$$F = \mathcal{M} - T_H \frac{A_H}{4}. \quad (3.27)$$

The situation of black objects in a grand canonical ensemble is also of interest, in which case we keep the temperature and the angular velocity of the horizon fixed. In this case, the thermodynamics is obtained from the Gibbs potential

$$W = \mathcal{M} - T_H \frac{A_H}{4} - (k+1) \Omega_H J. \quad (3.28)$$



Using the Smarr relation (3.25), one finds

$$W = \frac{\mathcal{M}}{d-2}. \quad (3.29)$$

Following the usual convention in the BRs/blackfold literature, we fix the overall scale of the solutions by fixing their mass  $\mathcal{M}$ . Then the solutions are characterized by a set of reduced dimensionless quantities, obtained by dividing out an appropriate power of  $\mathcal{M}$ :

$$j = c_j \frac{J}{\mathcal{M}^{\frac{d-2}{d-3}}}, \quad a_H = c_a \frac{A_H}{\mathcal{M}^{\frac{d-2}{d-3}}}, \quad w_H = c_w \Omega_H \mathcal{M}^{\frac{1}{d-3}}, \quad t_H = c_t T_H \mathcal{M}^{\frac{1}{d-3}}, \quad (3.30)$$

with the coefficients<sup>9</sup>

$$\begin{aligned} c_j &= \frac{(d-2)^{\frac{d-2}{d-3}}}{(16\pi)^{\frac{1}{d-3}} 2^{\frac{d-2}{d-3}}} \frac{1+k}{\sqrt{(d-3)(2k+1)}} (V_{(n+1)} V_{(2k+1)})^{\frac{1}{d-3}}, \\ c_a &= \frac{2^{\frac{2}{d-3}}}{(16\pi)^{\frac{d-2}{d-3}}} (d-2)^{\frac{d-2}{d-3}} \sqrt{\frac{d-2k-4}{d-3}} (V_{(n+1)} V_{(2k+1)})^{\frac{1}{d-3}}, \\ c_w &= \frac{2^{\frac{1}{d-3}}}{(d-2)^{\frac{1}{d-3}}} \sqrt{\frac{d-3}{2k+1}} \frac{(16\pi)^{\frac{1}{d-3}}}{(V_{(n+1)} V_{(2k+1)})^{\frac{1}{d-3}}}, \\ c_t &= \frac{(d-4)\sqrt{d-3}}{2^{\frac{2(d-2)}{d-3}} (d-2)^{\frac{1}{d-3}} (d-2k-4)^{\frac{3}{2}}} \frac{(16\pi)^{\frac{d-2}{d-3}}}{(V_{(n+1)} V_{(2k+1)})^{\frac{1}{d-3}}}. \end{aligned} \quad (3.31)$$

Finally, let us mention that all solutions possess an ergo-region, defined as the domain in which the metric function  $g_{tt}$  is positive. For the line element in this work, this domain is bounded by the event horizon and by the surface where

$$-f_0 + f_3 W^2 = 0. \quad (3.32)$$

### 3.5 Remarks on the numerics

Given the above framework, the only solutions of the Einstein equations which are known in closed form correspond to MP black holes with  $k+1$  equal angular momenta, and to the single spinning  $d=5$  Emparan-Reall BR (*i.e.* with  $k=0$ ). These configurations are discussed in the next Section.

All other solutions in this work are found by solving numerically the eqs. (3.5)-(3.10) within a nonperturbative approach. In our scheme, for given  $(d, k)$ , the only input parameters are  $R$ ,  $r_H$  and the angular velocity  $\Omega_H$ . (Note that although  $R$  and  $r_H$  have no invariant meaning, they provide a rough measure of the  $S^{n+1}$  and  $S^{2k+1}$  spheres, respectively, on the horizon.) Then all other quantities of interest, in particular the Hawking temperature  $T_H$ , the horizon area  $A_H$  and the global charges  $\mathcal{M}$ ,  $J$  are extracted from the numerical output, being encoded in the values of  $(f_i, W)$ .

---

<sup>9</sup>These coefficients are chosen such that to agree with those in [10] for  $k=0$ .

To find these functions, we employ a numerical algorithm developed in [16], [17], which uses a Newton-Raphson method whilst ensuring that all the Einstein equations are satisfied. In this approach, the functions  $f_i$  are expressed as products of suitable background functions  $f_i^{(0)}$  which possess the required behaviour on the boundaries, and unknown functions  $\mathcal{F}_i$ . The simplest choice for the background functions<sup>10</sup> of the solutions with a non-spherical horizon topology is given by  $F_1$ ,  $F_2$  and  $F_3$  in (2.12).

The advantage of this approach is that the coordinate singularities are essentially subtracted, while imposing at the same time the event horizon topology as well as the asymptotic structure of spacetime. The crucial point here is that the functions  $\mathcal{F}_i$  stay non-zero and finite everywhere. In particular, this holds on the boundaries, such that the behaviour of the solutions there remains as fixed by the background functions. The reader is referred to Ref. [17] for details of this procedure.

The equations for the  $\mathcal{F}_i, W$  result directly from (3.5)-(3.10) and are solved by using a finite difference solver [33]. This professional software provides an error estimate for each unknown function, which is the maximum of the discretization error divided by the maximum of the function. The typical numerical error for the solutions here is estimated to be lower than  $10^{-3}$ . (Note that we use an order six for the discretization of derivatives.) We have extensively tested the numerical results, including the convergence of the code for different resolutions of the mesh. Also, we have been able to recover  $d = 5$  balanced BRs and  $d = 5, 6$  MP black hole solutions with a single angular momentum, starting with the corresponding static configurations.

One should mention that we have constructed the  $d = 6$  BRs independently by using a multi-domain spectral solver. Here the functions are expanded in products of Chebychev polynomials. The resulting systems of algebraic equations for the expansion coefficients are then solved with the Newton-Raphson method. The iteration matrix of the ‘linear problem’ is no longer sparse and is solved by Gaussian elimination. We have found a very good agreement for the results obtained by these two different numerical schemes.

For both approaches, another kind of test of the numerics is provided by the Smarr relation (3.25) and by the 1<sup>st</sup> law (3.26). The typical relative errors found in this way are  $< 10^{-3}$ . A further numerical test is provided by the constraint equations,  $G_r^\theta = 0$  and  $G_r^r - G_\theta^\theta = 0$ , which in our scheme are not solved directly. However, usually these constraints are satisfied with the same order of the relative error as the Smarr relation.

## 4. Exact solutions

### 4.1 A spherical horizon topology: the Myers-Perry black holes

The simplest solutions of the eqs. (3.5)-(3.10) correspond to the MP solutions with  $k+1$  equal

---

<sup>10</sup>However, we have found that a choice for  $f_i^{(0)}$  corresponding to the functions which enter the  $d = 5$  static BR leads to better results. In this case,  $f_1^{(0)}$ ,  $f_2^{(0)}$  and  $f_3^{(0)}$  are essentially  $F_1$ ,  $F_2$  and  $F_3$  in (3.1), though with some  $r_H$ -dependent corrections which are finite and nonzero everywhere. Most of the numerical results reported in this work have been found for this choice of  $f_i^{(0)}$ .

angular momenta.

A convenient expression of the metric functions  $f_i$  which enter (3.1) is

$$\begin{aligned} f_0(r, \theta) &= \frac{\Delta(r)}{(r^2 + a^2)P(r, \theta)}, \quad f_1(r, \theta) = \frac{r^2 + a^2 \cos^2 \theta}{\Delta(r)}, \quad f_2(r, \theta) = r^2 \cos^2 \theta, \\ f_3(r, \theta) &= (r^2 + a^2) \sin^2 \theta P(r, \theta), \quad f_4(r, \theta) = (r^2 + a^2) \sin^2 \theta, \\ W(r, \theta) &= \frac{M}{r^{d-(2k+5)}} \frac{a}{(r^2 + a^2)^{k+1} (r^2 + a^2 \cos^2 \theta) P(r, \theta)}, \end{aligned} \quad (4.1)$$

where

$$\begin{aligned} \Delta(r) &= (r^2 + a^2) \left( 1 - \frac{M}{r^{d-(2k+5)} (r^2 + a^2)^{k+1}} \right), \\ P(r, \theta) &= 1 + \frac{M}{r^{d-(2k+5)}} \frac{a^2 \sin^2 \theta}{(r^2 + a^2)^{k+1} (r^2 + a^2 \cos^2 \theta)}, \end{aligned} \quad (4.2)$$

while  $M, a$  are two input parameters<sup>11</sup>. To give an idea about these functions in contrast to the ring(oid) case, we exhibit in Figure 3 the profiles of a typical  $d = 7, k = 1$  configuration. The Kretschmann scalar  $K = R_{\mu\nu\alpha\beta} R^{\mu\nu\alpha\beta}$  is also shown there (note that a straightforward computation shows that  $K$  is finite everywhere, in particular at  $r = r_H, \theta = \pi/2$ ).

These black holes have a horizon of spherical topology located at  $r = r_H$ , where  $\Delta(r_H) = 0$ , which implies

$$M = (r_H^2 + a^2)^{k+1} r_H^{d-(2k+5)}. \quad (4.3)$$

The quantities of interest which enter the thermodynamics of these solutions are given by

$$\begin{aligned} \mathcal{M} &= \frac{(d-2)V_{(d-2)}r_H^{d-2k-5}}{16\pi} (r_H^2 + a^2)^{k+1}, \quad J = \frac{V_{(d-2)}}{8\pi} a r_H^{d-2k-5} (r_H^2 + a^2)^{k+1}, \\ A_H &= V_{(d-2)} r_H^{d-2k-4} (r_H^2 + a^2)^{k+1}, \quad T_H = \frac{1}{4\pi r_H} \left( d - 3 - \frac{2a^2(k+1)}{a^2 + r_H^2} \right), \quad \Omega_H = \frac{a}{a^2 + r_H^2}. \end{aligned} \quad (4.4)$$

This implies the following relations for the scaled dimensionless quantities as defined by (3.30):

$$\begin{aligned} j &= q_j \frac{x}{(1+x^2)^{\frac{k+1}{d-3}}}, \quad a_H = q_a \frac{1}{(1+x^2)^{\frac{k+1}{d-3}}}, \\ t_H &= q_t \frac{(d-2k-5)x^2 + d-3}{(1+x^2)^{\frac{d-k-4}{d-3}}}, \quad w_H = q_w \frac{x}{(1+x^2)^{\frac{d-k-4}{d-3}}}, \end{aligned} \quad (4.5)$$

---

<sup>11</sup>Note that, when written in this form the near horizon expression of the solutions differs from (A.1), (A.2). The relations (A.1), (A.2) are recovered by working with a different radial coordinate. However, the expression of the solution looks much more complicated in that case.

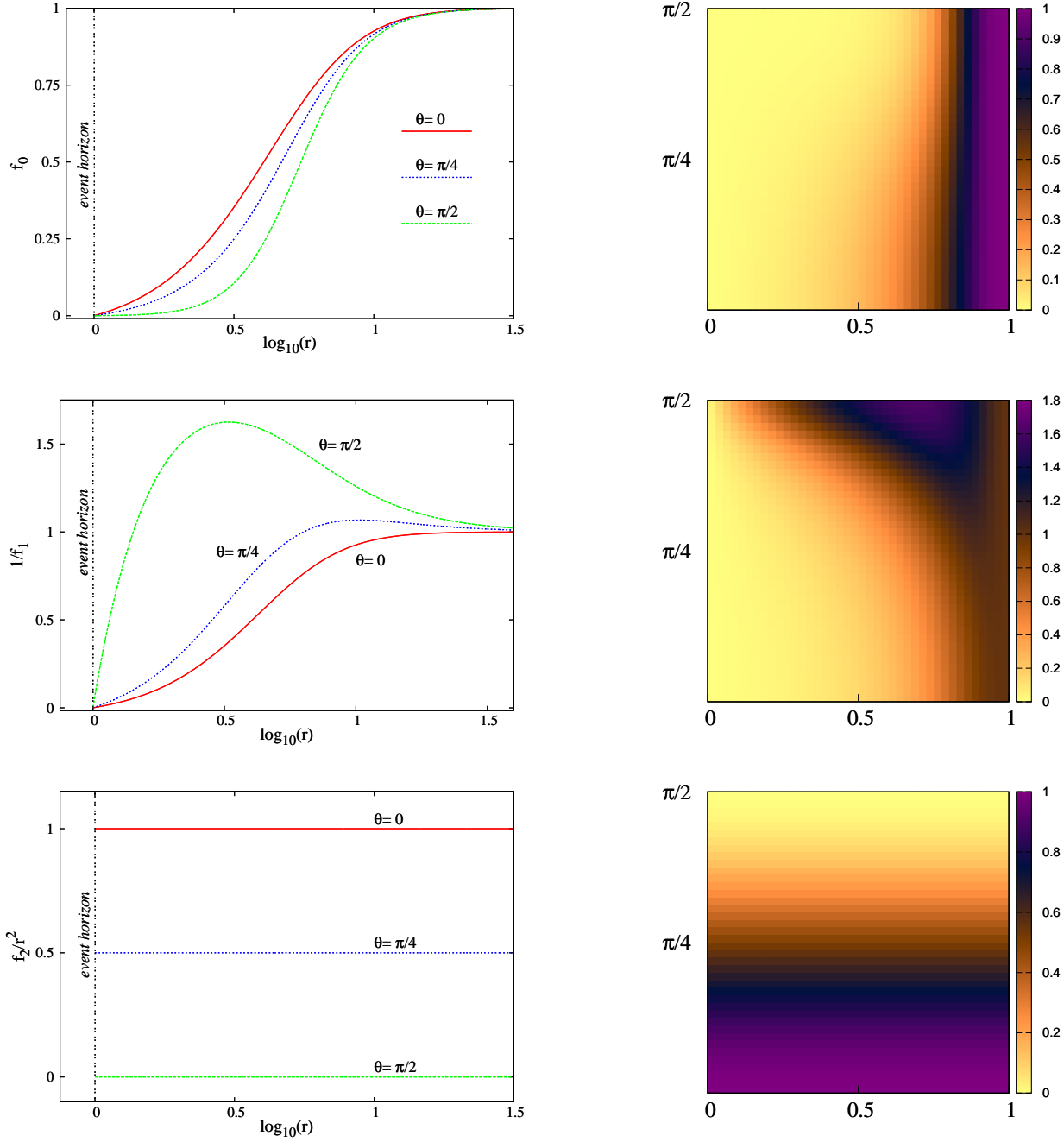


**Figure 3:** The metric functions  $f_i, W$  and the Kretschmann scalar  $K = R_{\mu\nu\alpha\beta}R^{\mu\nu\alpha\beta}$  are shown for a  $d = 7$ ,  $k = 1$  Myers-Perry black hole with the input parameters  $r_H = 1$  and  $\Omega_H \simeq 0.162$ . Here and in Figures 4, 8 and 13 the left panels show the profiles for several angles  $\theta$ ; the right panels are colour maps of the same functions in terms of  $(x = 1 - r_H/r, \theta)$ , which should be viewed together with the diagrams in Fig. 2.

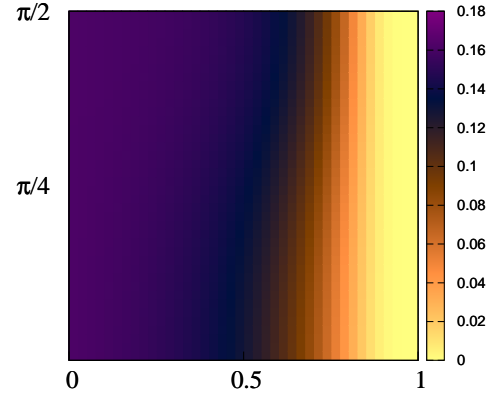
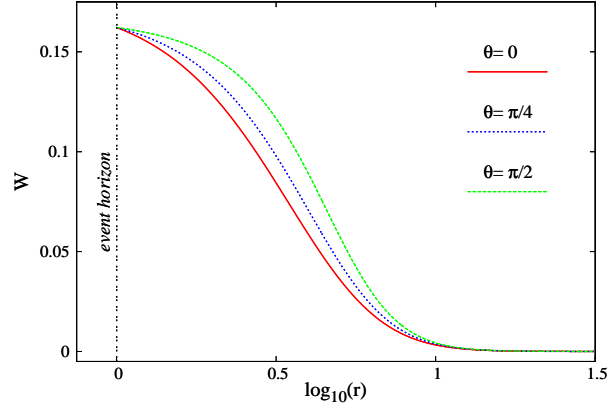
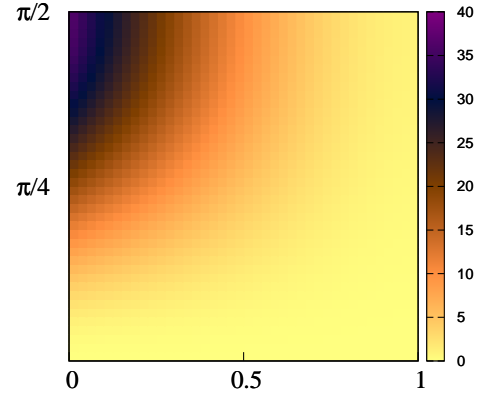
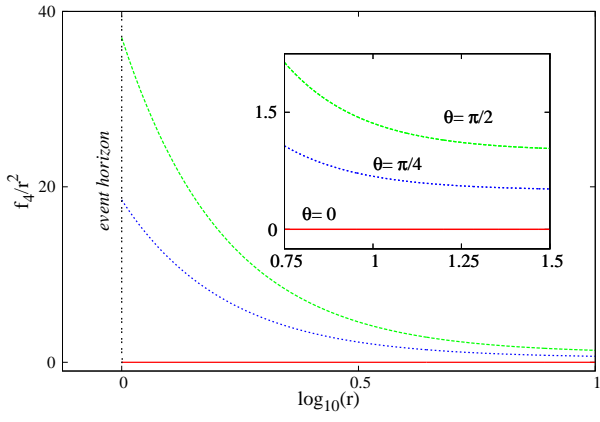
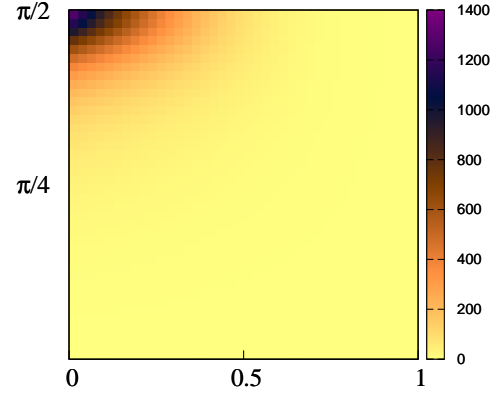
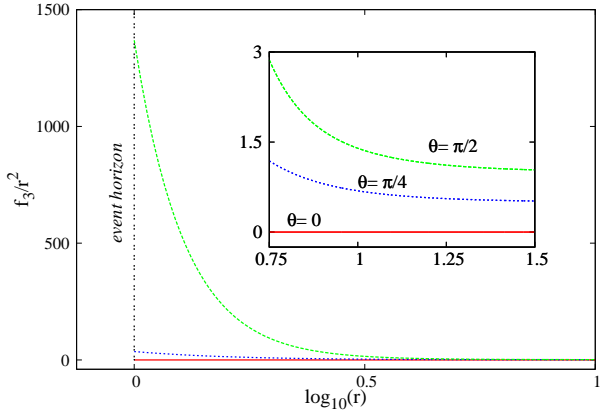
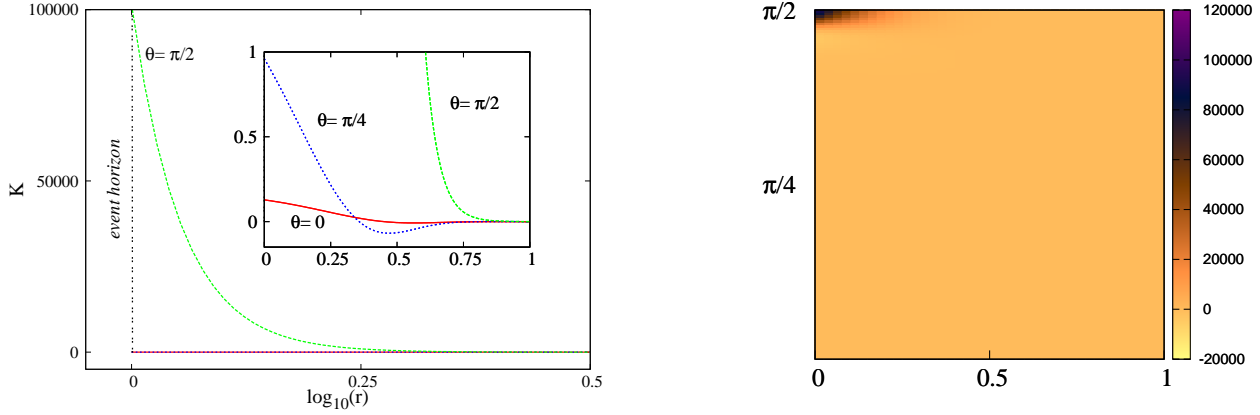


Figure 3: continued.

with

$$x = \frac{a}{r_H}, \quad 0 \leq x < \infty, \quad (4.6)$$



**Figure 3:** continued.

and the coefficients:

$$\begin{aligned}
 q_j &= \frac{(k+1)\pi^{\frac{1}{2(d-3)}}}{\sqrt{(d-3)(2k+1)}} \left( \frac{\Gamma(\frac{d-1}{2})}{\Gamma(\frac{d}{2} - (k+1))k!} \right)^{\frac{1}{d-3}}, \\
 q_a &= \frac{2^{\frac{2}{d-3}} \pi^{\frac{1}{2(d-3)}}}{\sqrt{\frac{d-3}{d-2k-4}}} \left( \frac{\Gamma(\frac{d-1}{2})}{\Gamma(\frac{d}{2} - (k+1))k!} \right)^{\frac{1}{d-3}}, \\
 q_w &= \frac{1}{\pi^{\frac{1}{2(d-3)}}} \sqrt{\frac{d-3}{2k+1}} \left( \frac{\Gamma(\frac{d-1}{2})}{\Gamma(\frac{d}{2} - (k+1))k!} \right)^{\frac{1}{d-3}}, \\
 q_t &= \frac{1}{2^{\frac{3}{d-3}}} \frac{1}{\pi^{2(d-3)}} \frac{(d-4)\sqrt{d-3}}{(d-2k-4)^{\frac{3}{2}}} \left( \frac{\Gamma(\frac{d-1}{2})}{\Gamma(\frac{d}{2} - (k+1))k!} \right)^{\frac{1}{d-3}}.
 \end{aligned} \tag{4.7}$$

From the above relations it is clear that the odd-dimensional case with  $n = 1$ , *i.e.*

$$d = 2k + 5 \tag{4.8}$$

is special. It is the only case where extremality is possible (which is reached for  $x \rightarrow \infty$ ) and the angular momentum is bounded from above. The extremal solutions of this class share the properties of the  $d = 5$  extremal MP black holes with a single  $J$  ( $k = 0$ ). In particular, the event horizon has a vanishing area. The near horizon geometry of the extremal solutions is described by the following line element<sup>12</sup>

$$ds^2 = \cos^2 \theta \left( -\frac{r^2}{a^2} dt^2 + \frac{a^2}{r^2} dr^2 + r^2 d\phi^2 \right) + \frac{(d-3)}{2} a^2 \left( \cos^2 \theta d\theta^2 + \tan^2 \theta (d\psi + \mathcal{A})^2 + \sin^2 \theta d\Sigma_k^2 \right), \tag{4.9}$$

<sup>12</sup>The case  $d = 5$ ,  $k = 0$  is discussed in [34].

which solves the Einstein equations. Thus it turns out that the properties of the five dimensional solutions are generic, with (4.9) representing a singular geometry for any value of  $k$ .

The situation is different for MP solutions with  $n > 1$ , since in this case the properties are similar to those of the (better known)  $d > 5$  MP black holes with a single angular momentum. Here the angular momenta do not possess an upper bound, while  $a_H, t_H$  are strictly positive quantities. Thus these black holes possess an ultraspinning regime, which is described by the corresponding blackfolds, see the discussion in Section 5.1.

## 4.2 The $d = 5$ Emparan-Reall black ring

Despite various attempts, the  $d = 5$  Emparan-Reall BR (and its Pomeransky-Sen'kov generalization [44]) remains the only asymptotically flat vacuum (single) black object with a nonspherical topology of the horizon which is known in closed form. In all studies, this solution is written in (some version of) ring coordinates, or in Weyl coordinates. However, the BR can also be studied by using the framework introduced in the previous Section.

The line element is found by taking  $k = 0, d = 5$  in (3.1) and reads

$$ds^2 = f_1(r, \theta)(dr^2 + r^2 d\theta^2) + f_2(r, \theta)d\phi^2 + f_3(r, \theta)(d\psi - W(r, \theta)dt)^2 - f_0(r, \theta)dt^2. \quad (4.10)$$

The expression of the metric functions  $f_i, W$  is given in Appendix B, together with the corresponding expansion at  $r = r_H, \infty$  and  $\theta = 0, \pi/2$ , respectively. The profiles of a typical solution are given in Figure 4; for completeness and comparison with the higher dimensional case, we show there also the Kretschmann scalar  $K = R_{\mu\nu\alpha\beta}R^{\mu\nu\alpha\beta}$  of the same solution.

The quantities which enter the thermodynamics of the  $d = 5$  BRs exhibit a complicated dependence on the input parameters  $(R, r_H)$ :

$$\begin{aligned} A_H &= \frac{32\pi^2 \sqrt{2} R r_H^4 \sqrt{R^4 + r_H^4}}{(R^2 - r_H^2)^2}, \quad T_H = \frac{(R^2 - r_H^2)^2}{8\pi \sqrt{2} R r_H^2 \sqrt{R^4 + r_H^4}}, \quad \Omega_H = \frac{R(R^2 - r_H^2)}{\sqrt{2}(R^2 + r_H^2) \sqrt{R^4 + r_H^4}}, \\ M &= \frac{3\pi r_H^2 (R^4 + r_H^4)}{(r^2 - r_H^2)^2}, \quad J = \frac{\sqrt{2}\pi r_H^2 (R^2 + r_H^2)^3 \sqrt{R^4 + r_H^4}}{R(R^2 - r_H^2)^3}, \end{aligned} \quad (4.11)$$

while for the quantities which encode the deformation of the horizon one finds

$$\begin{aligned} L_e &= \frac{4\pi r_H^2 R}{\sqrt{R^4 + r_H^4}}, \quad L_p = \frac{8R r_H^2}{R^2 - r_H^2} E\left(\frac{4R^2 r_H^2}{(R^2 + r_H^2)^2}\right), \\ R_1^{(in)} &= \frac{\sqrt{2}\sqrt{R^4 + r_H^4}}{R}, \quad R_1^{(out)} = \frac{\sqrt{2}(R^2 + r_H^2)^2 \sqrt{R^4 + r_H^4}}{R(R^2 - r_H^2)^2}. \end{aligned} \quad (4.12)$$

with  $E(x)$  the complete elliptic integral of the second kind.

Detailed discussions of the properties of this solution have appeared in various places in the literature, see *e.g.* the review work [25]. Here we shall briefly mention only some features which occur later when discussing the numerical solutions.

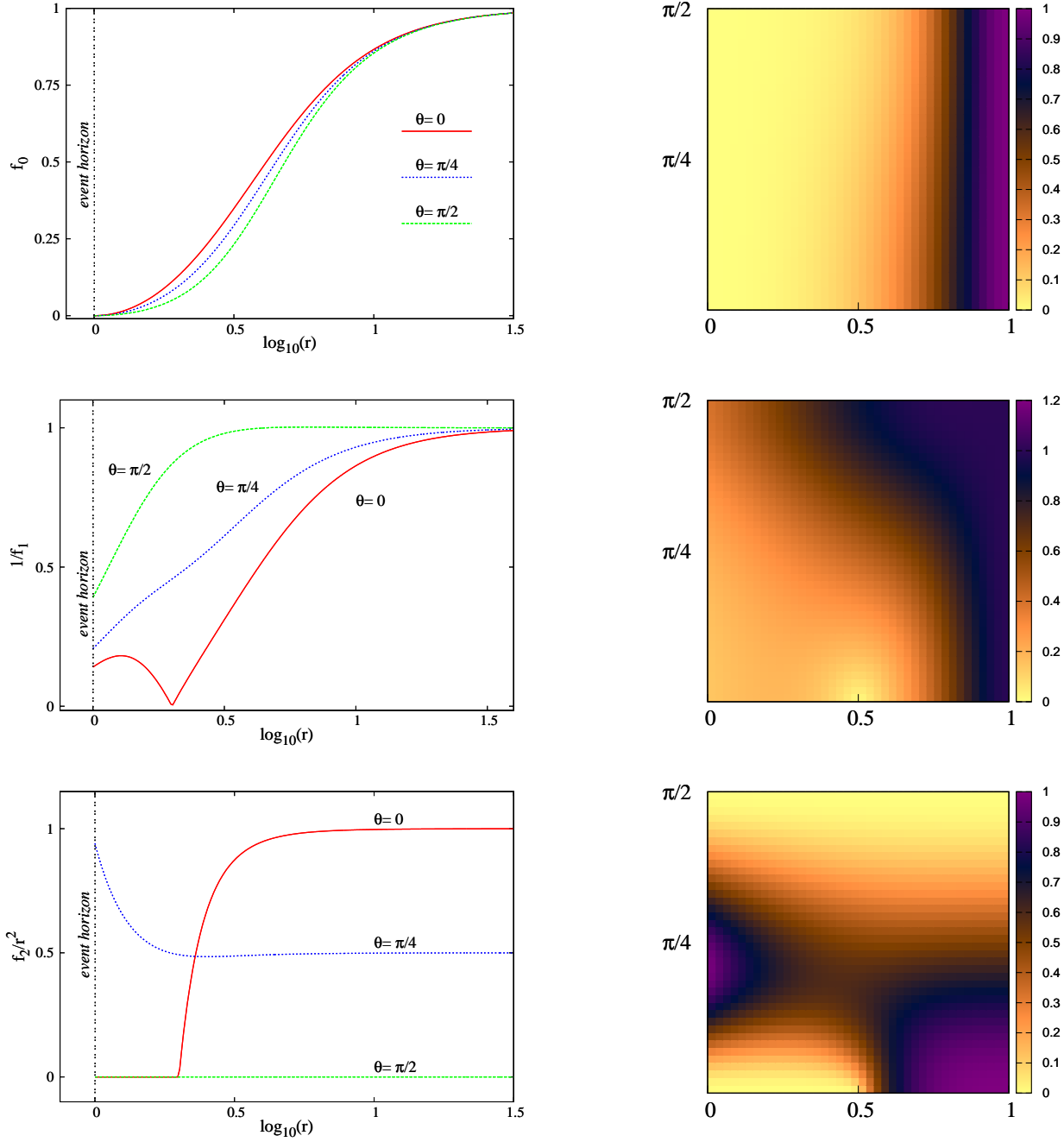


**Figure 4:** The metric functions  $f_i, W$  and the Kretschmann scalar  $K = R_{\mu\nu\alpha\beta}R^{\mu\nu\alpha\beta}$  are shown for a  $d = 5$  Emparan-Reall black ring with  $r_H = 1$ ,  $R = 2$  and  $\Omega_H \simeq 0.205$ .

Let us start by observing that the expression above (including those in Appendix B) hold for a balanced BR. However, unbalanced solutions exist as well, possessing one more free



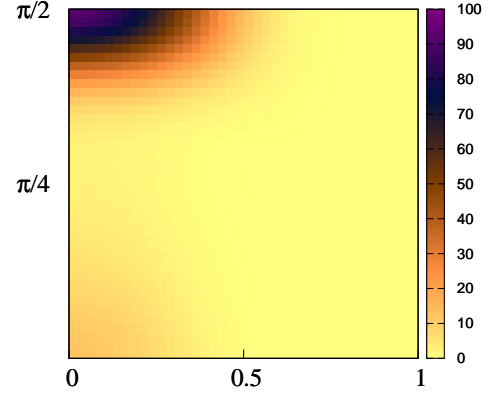
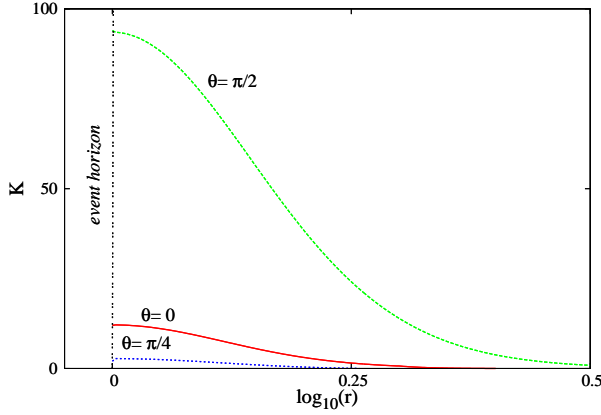
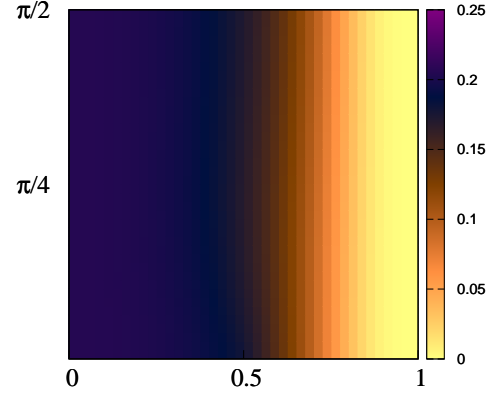
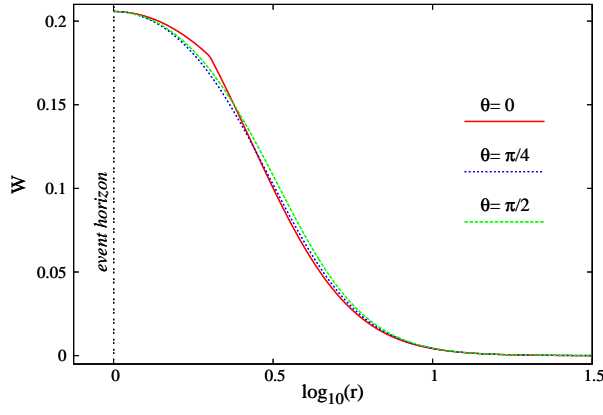
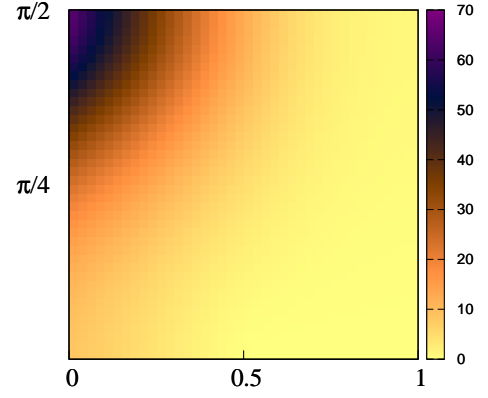
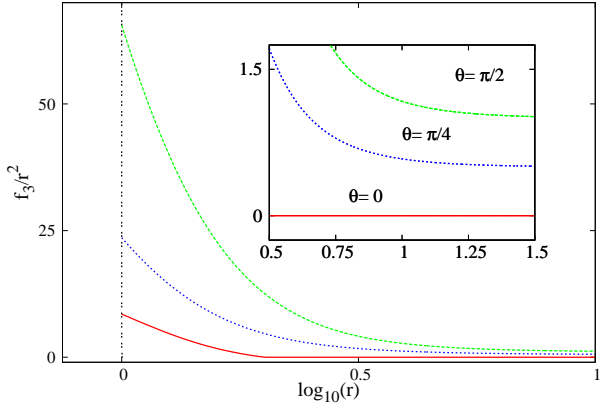
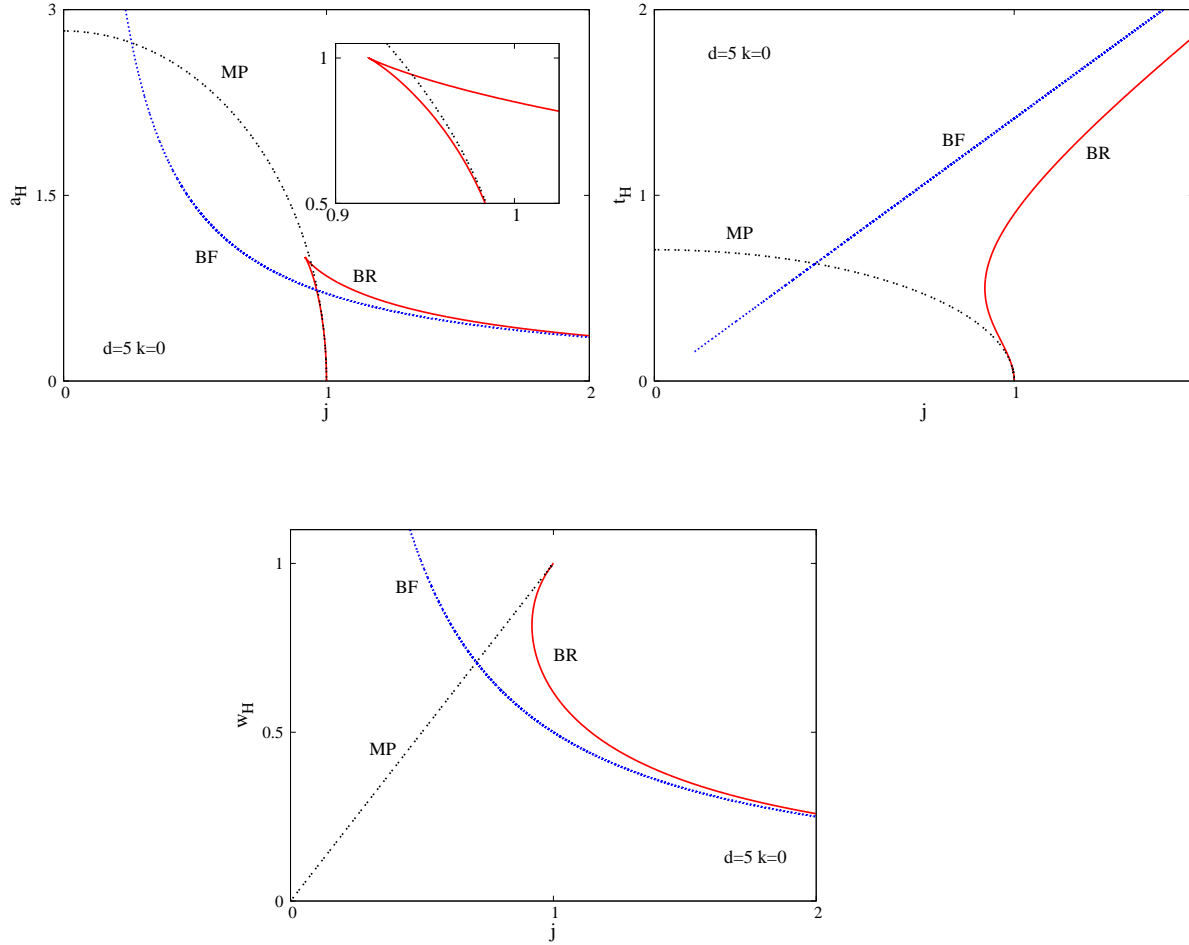


Figure 4: continued.

parameter. That is, for given  $(r_H, R)$ , BRs without conical singularities are found for a single value of  $\Omega_H$  only, as given by (4.11). Also, the BRs with  $R \gg r_H$  (and thus, from (4.11), with large  $J$ ) effectively become boosted black strings, being well described by the blackfold



**Figure 5.** The reduced area  $a_H$ , the reduced temperature  $t_H$  and the reduced angular velocity  $w_H$  are shown *vs.* the reduced angular momentum  $j$  for  $d = 5$  black rings (BR) and Myers-Perry (MP) black holes. For comparison with the higher dimensional case, we include here also the lowest order blackfold (BF) prediction.

formalism. (Note that the angular momentum of the BR (for fixed mass) is bounded below, but not above.)

However, perhaps the most unexpected feature of the BRs is the existence of two branches, which branch off from a cusp at  $(j^2, a_H) = (27/32, 1)$ . The existence and the properties of the branch of ‘fat’ BRs cannot be predicted by the blackfold approach. It has a small extent, meeting at  $(j^2, a_H) = (1, 0)$  the  $k = 0$ ,  $d = 5$  singular MP solution.

These features are shown in Figure 5; although these plots can be found in the literature, we have included them here since it is interesting to contrast the situation with the higher dimensional case.

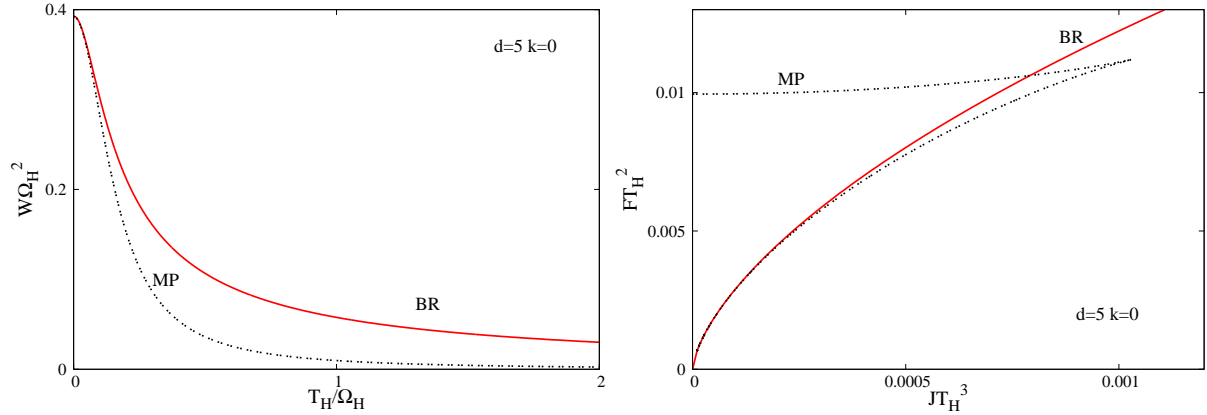


**Figure 6.** *Left:* The grand canonical potential  $W$  is shown as a function of the Hawking temperature  $T_H$  for  $d = 5$  black rings (BR) and Myers-Perry (MP) black holes with fixed angular velocity of the horizon  $\Omega_H$ . *Right:* The canonical potential  $F$  is shown as a function of the angular momentum  $J$  for  $d = 5$  black rings with fixed Hawking temperature  $T_H$ .

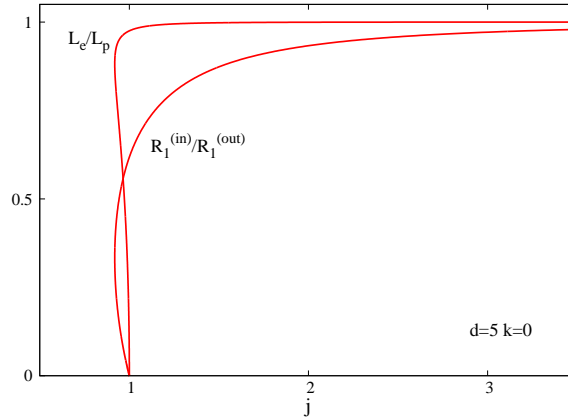


**Figure 7.** The ratios  $L_e/L_p$  and  $R_1^{(in)}/R_1^{(out)}$ , which encode the deformation of the horizon, are shown *vs.* the reduced angular momentum  $j$  for  $d = 5$  black ring solutions.

The behaviour of the solutions in a grand canonical ensemble is shown in Figure 6 (left). One can notice the existence of only one BR and one MP black hole with the same values of  $\Omega_H$  and  $T_H$ . Moreover, the solutions exist for all possible values of these variables. Also, as discussed in [35], in a grand canonical potential the MP black holes are always thermodynamically favoured over the BRs<sup>13</sup>.

<sup>13</sup>This results from the fact that, for given  $T_H$ ,  $\Omega_H$ , the grand canonical potential  $W$  is minimized by the MP black holes.

As seen in Figure 6 (right), a different picture is found for the same black objects in a canonical potential. The MP black holes exhibit in this case two branches, with a ‘swallow-tail’ structure, while only one branch of solutions is found for the BRs. Note that in the region of co-existence, the potential  $F$  is minimized by a MP solution, which is therefore thermodynamically preferred. Also, at  $(JT_H^3 \simeq 0.00079, FT_H^2 \simeq 0.0106)$  the two curves meet and only BRs exist for large  $J$  (at fixed  $T_H$ ).

Finally, in Figure 7 we show the ratios  $L_e/L_p$  and  $R_1^{(in)}/R_1^{(out)}$  (as defined by (3.22) and (3.23), respectively), which encode the deformation of the horizon, *vs.* the reduced angular momentum  $j$ . There one can see *e.g.* that the hole inside the ring shrinks to zero size while the outer radius goes to infinity as the singular solution is approached.

## 5. Black objects with non-spherical horizon topology

### 5.1 The blackfold limit

The ultraspinning limit of the black objects with  $S^{n+1} \times S^{2k+1}$  horizon topology has been already discussed in the blackfold literature, see *e.g.* [13]. The results there imply the following expressions for the reduced quantities, valid to leading order:

$$a_H = \frac{1}{2^{\frac{d(2k-1)+6}{(d-2k-4)(d-3)}}} \frac{1}{j^{\frac{2k+1}{d-2k-4}}}, \quad t_H = (d-4)2^{\frac{d(2k-1)+6}{(d-2k-4)(d-3)}} j^{\frac{2k+1}{d-2k-4}}, \quad w_H = \frac{1}{2j}. \quad (5.1)$$

The corresponding relations for the ultraspinning MP black holes with  $n > 1$  are also of interest:

$$a_H = q_a q_j^{\frac{2(k+1)}{d-2k-5}} \frac{1}{j^{\frac{2(k+1)}{(d-2k-5)}}}, \quad t_H = \frac{(d-2k-5)q_t}{q_j^{\frac{2(k+1)}{(d-2k-5)}}} j^{\frac{2(k+1)}{(d-2k-5)}}, \quad w_H = \frac{q_j q_w}{j}, \quad (5.2)$$

with the coefficients  $q_a$ ,  $q_j$ ,  $q_w$  given by (4.7) (note also that the product  $a_H t_H$  is constant in both cases).

From the above relations one can see that the area decreases faster for MP black holes than for the BRs/ringoids. That is, the black objects with a  $S^{n+1} \times S^{2k+1}$  horizon topology dominate entropically in the ultraspinning regime.

### 5.2 Non-perturbative solutions

#### 5.2.1 $k = 0$ : black rings in $d = 6$ dimensions

Let us start with the simplest case,  $k = 0$ , corresponding to BRs with rotation on the  $S^1$ . The only dimension we have studied so far in a more systematic way is  $d = 6$ .

A discussion of the basic properties of these solutions has been given already in Ref. [18]; here we return with a more detailed description. Let us also mention that, recently these solutions have been constructed independently in [20]. Although the results there have been

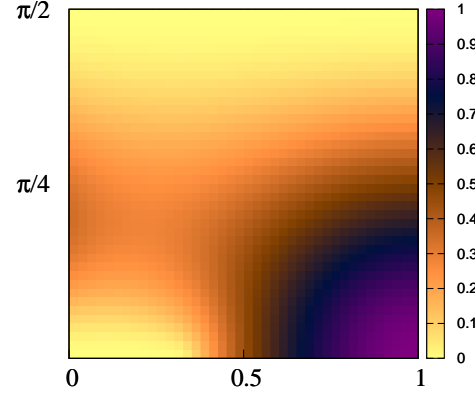
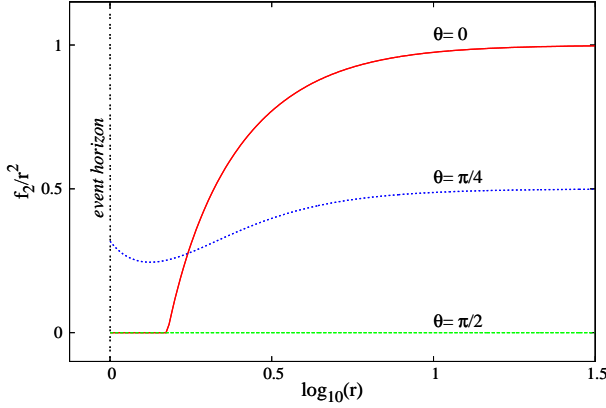
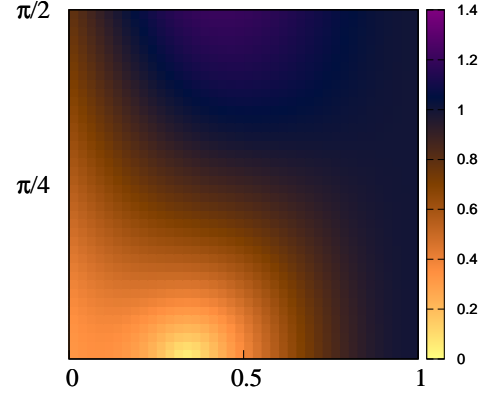
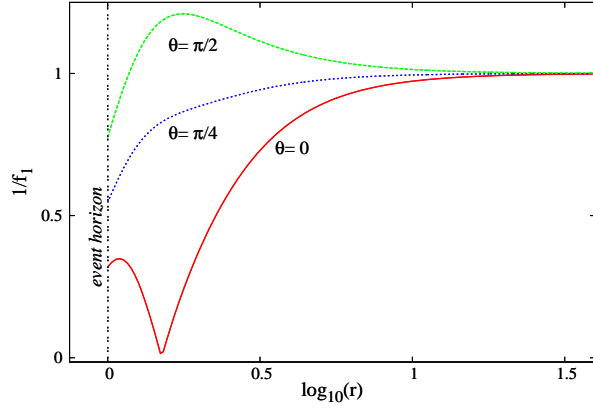
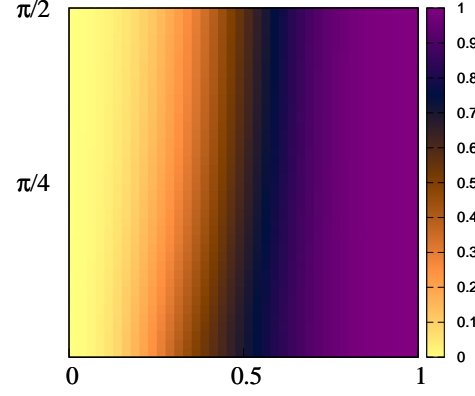
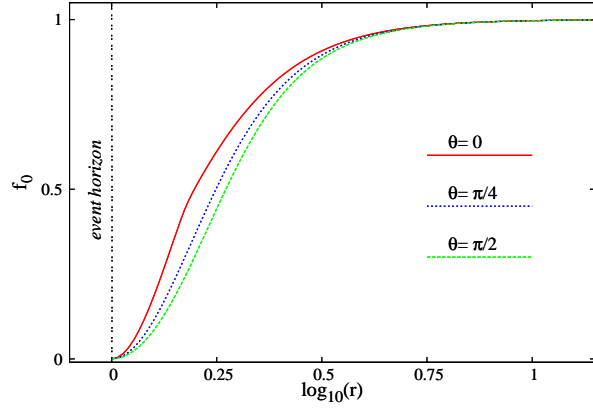


**Figure 8:** The metric functions  $f_i$ ,  $W$  and the Kretschmann scalar  $K = R_{\mu\nu\alpha\beta}R^{\mu\nu\alpha\beta}$  are shown for a  $d = 6$  black ring with the input parameters  $r_H = 1$ ,  $R = 1.504$ ,  $\Omega_H \simeq 0.352$ .

found by using a very different approach<sup>14</sup> as compared to the one described above, they

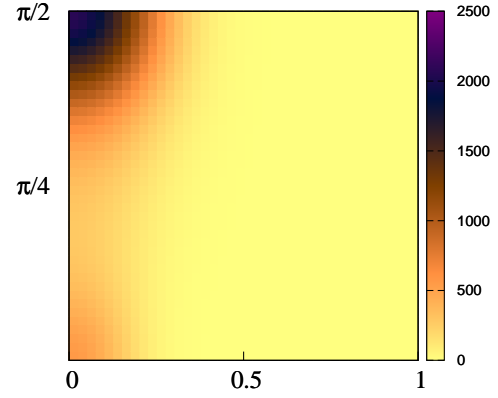
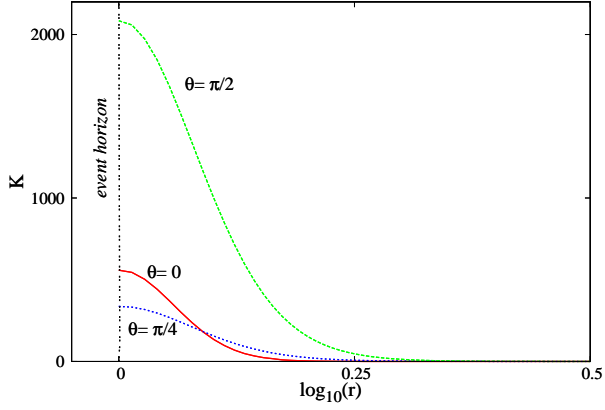
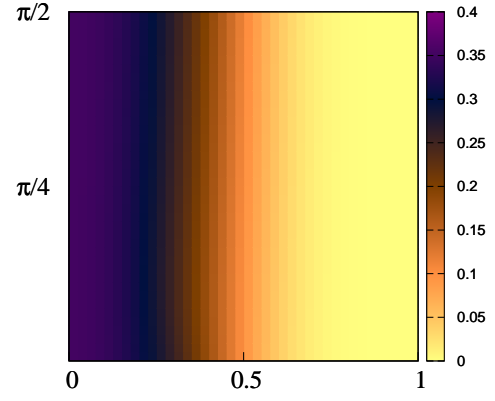
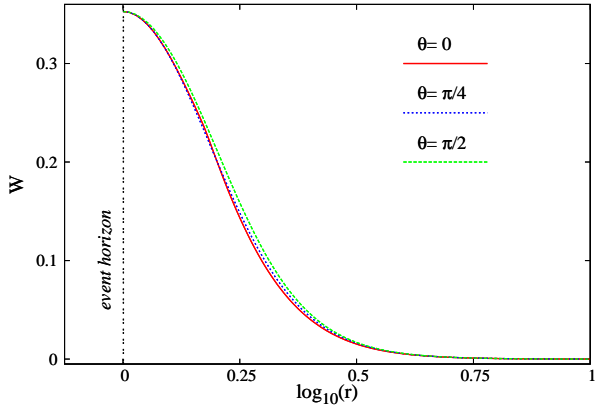
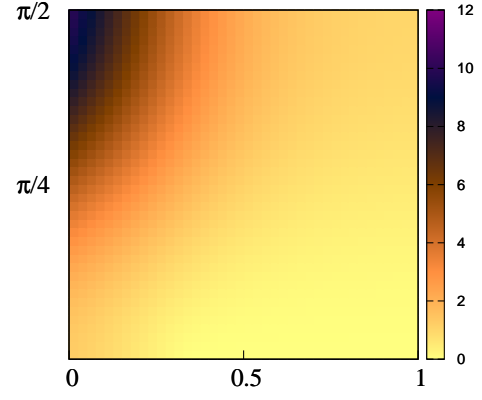
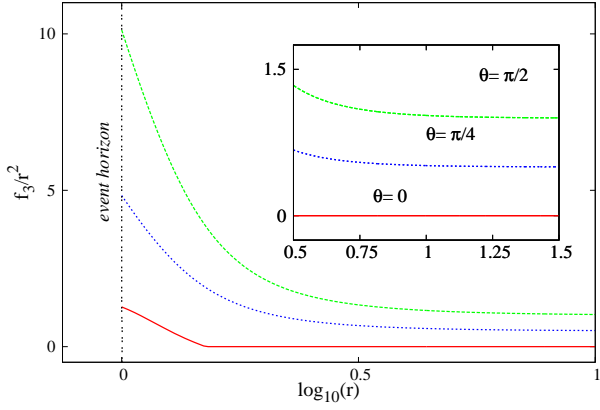
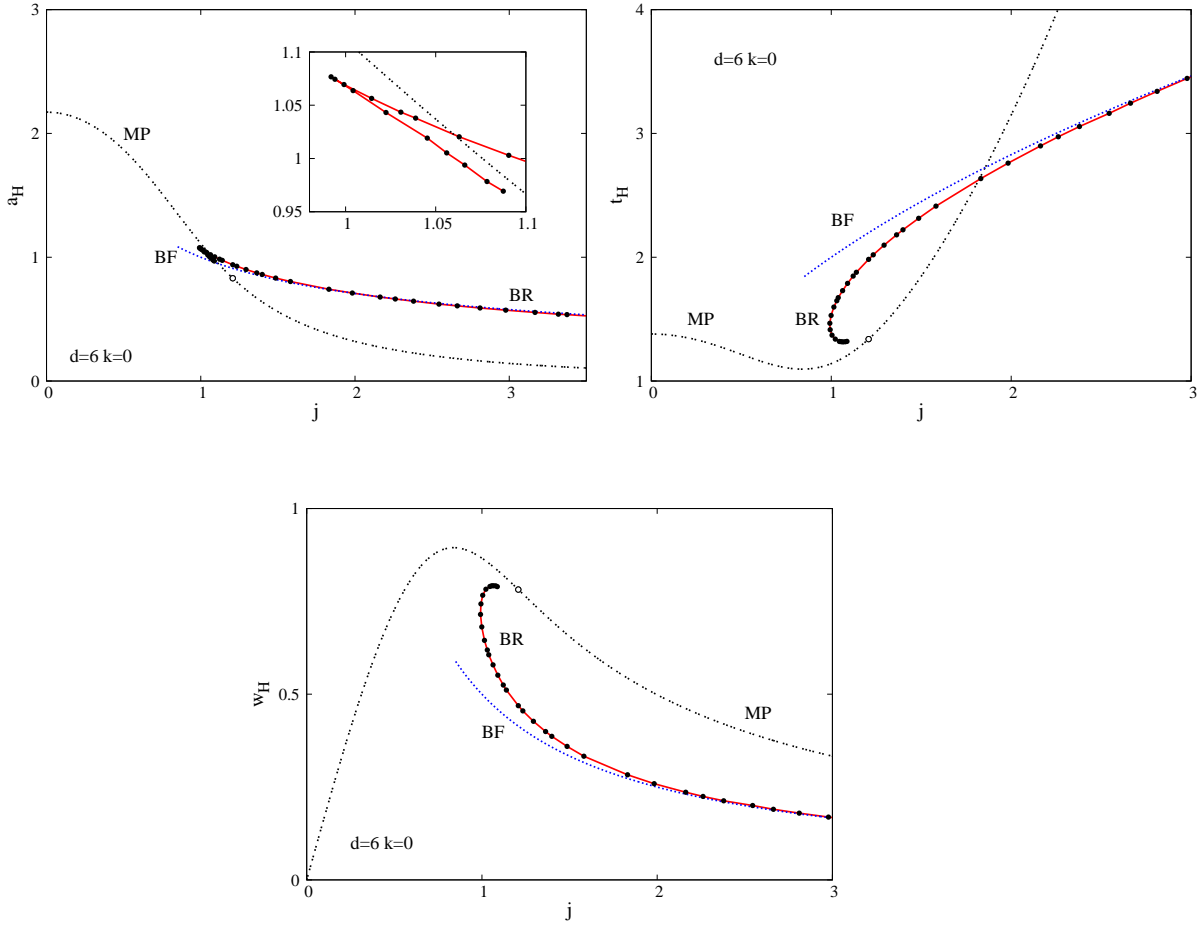


Figure 8: continued.

agree well with those reported in [18].

<sup>14</sup>For example, the Ref. [20] uses a ring-like coordinate system. Also, the Einstein equations are solved by using the DeTurck method [36].



**Figure 9.** The reduced area  $a_H$ , the reduced temperature  $t_H$  and the reduced angular velocity  $w_H$  are shown *vs.* the reduced angular momentum  $j$  for  $d = 6$  black rings (BR) and Myers-Perry (MP) black holes with a single angular momentum. The blackfold (BF) prediction for the black rings is also shown. Here and in Figure 10, the circle on the MP curve indicates the critical solution where the branches of pinched black holes emerge.

The numerical scheme described in Section 3 requires a further adjustment for  $d > 5$  BRs. In five dimensions, BRs exist for arbitrary values of  $\Omega_H$ , generically possessing conical singularities.

Only for a critical value of the event horizon velocity a BR becomes balanced [4]. We have found that the situation is different for  $d > 5$ , since the singularities of the unbalanced configurations are stronger in this case<sup>15</sup>. That is, for given  $R$ ,  $r_H$  and arbitrary  $\Omega_H$ , the numerical algorithm diverges, which we take as an indication for the occurrence of singularities,

<sup>15</sup>This is not an unexpected feature; indeed, the analysis in [10] predicts the occurrence of naked singularities for  $d > 5$  BRs which do not satisfy the equilibrium condition.

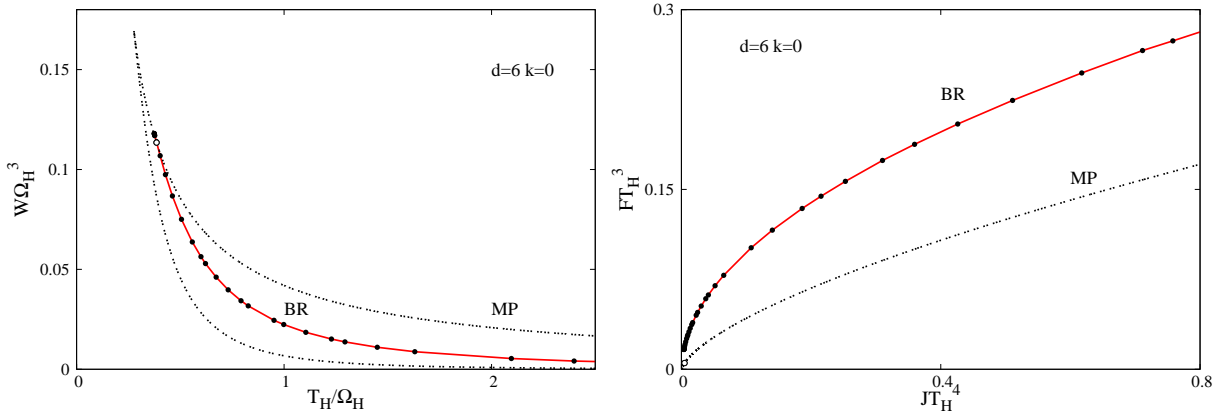


**Figure 10.** *Left:* The grand canonical potential  $W$  is shown as a function of the Hawking temperature  $T_H$  for  $d = 6$  black rings (BR) and Myers-Perry (MP) black holes with fixed angular velocity of the horizon  $\Omega_H$ . *Right:* The canonical potential  $F$  is shown as a function of the angular momentum  $J$  for the same configurations with fixed Hawking temperature  $T_H$ .

a situation that cannot be dealt with in our scheme. However, the numerical errors decrease dramatically for some (small) range of  $\Omega_H$  and the solver starts to converge. The critical value of the event horizon velocity, where the ring is precisely balanced, is found by using a shooting procedure in terms of  $\Omega_H$ . Then the balanced solution has no singularity on and outside the horizon. This can be seen by computing the Kretschmann scalar which is finite everywhere.

Therefore, in principle, by varying the value of  $R$  for fixed  $r_H$  and by adjusting the value of  $\Omega_H$  via a shooting algorithm, the full spectrum of  $d = 6$  balanced BRs can be recovered numerically.

We have studied in a systematic way the  $d = 6$  BR solutions with  $1.12r_H < R < 7r_H$ . However, we could not obtain BRs closer to the critical point  $R = r_H$  with high accuracy, although we have a strong indication for their existence.

The profiles for the metric functions  $f_i, w$  are rather similar to those of the  $d = 5$  balanced BR solution, a typical configuration being shown in Fig. 8. To illustrate the regular character of the solution, we plot there also the Kretschmann scalar.

The general picture we have unveiled for  $d = 6$  BRs exhibits a number of similarities to the well-known  $d = 5$  case. Again, one finds two branches of BR solutions whose physical differences are most clearly seen in terms of the reduced quantities  $a_H$  and  $j$  introduced in Section 3. The  $a_H(j)$  diagram of the BRs is shown in Figure 9, where the singly rotating MP BHs are included as well. There we show also the dependence of the reduced temperature  $t_H$  and the reduced horizon angular velocity  $w_H$  on the reduced angular momentum  $j$ . The analytical curve corresponding to the blackfold prediction is also included in those plots.



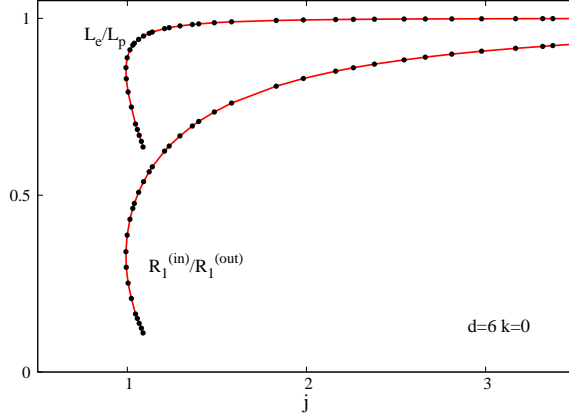


**Figure 11.** The ratios  $L_e/L_p$  and  $R_1^{(in)}/R_1^{(out)}$ , which encode the deformation of the horizon, are shown *vs.* the reduced angular momentum  $j$  for  $d = 6$  black ring solutions.

These diagrams clearly show that the nonuniqueness result in five dimensions [4] extends also to the  $d = 6$  case. We observe that the reduced area  $a_H(j)$  has a cusp at a minimal value of  $j$ ,  $j_{\min}^{(BR)} \simeq 0.991$ , where  $a_H$  assumes its maximal value,  $a_H \simeq 1.076$ . Starting from this cusp the upper branch of solutions extends to  $j \rightarrow \infty$ . Our results show that in the ultraspinning regime, these BRs are very well approximated by boosted black strings. In fact, we have found that the blackfold analytical result provides a good approximation for spinning  $d = 6$  solutions with  $j \gtrsim 2$  (which include also a set of ‘not-so fast’ spinning rings).

In agreement with the  $d = 5$  picture, starting from the cusp there is also a lower branch of BRs, the branch of ‘fat’ BRs. (Note that this feature is not predicted by the blackfold results.) Thus, in a certain range of the reduced angular momentum  $j_{\min}^{(BR)} < j < j_{\max}$  there exist three different solutions with the same global charges.

This lower branch have a small extent in both  $j$  and  $a_H$ , ending in a critical merger configuration [10], where a branch of ‘pinched’ black holes is approached in a horizon topology changing transition. Extrapolations of the present data together with the results in the recent work [20] indicate that the critical configuration might be in the vicinity of  $j_{\max} \simeq 1.14$ ,  $a_H \simeq 0.918$  and  $t_H \simeq 1.34$ . The numerical results here and those in [20] clearly show that the critical merger solution has a finite, nonzero area, while the temperature stays also finite and thus nonzero. This critical behaviour of the  $d = 6$  BRs is in strong contrast with the one of the  $d = 5$  BRs [4], where the branch of ‘fat’ BRs merges with the MP black hole branch in a singular solution with  $j = 1$ ,  $a_H = 0$  and  $t_H = 0$ .

The results in [20] show that the  $d = 6$  ‘pinched’ black holes branch off from a critical MP black hole solution at  $j \simeq 1.27$ ,  $a_H \simeq 0.83$ , along the stationary zero-mode perturbation of the GL-like instability [21, 22]. (In fact, a more complicated picture is unveiled there, showing the existence of two branches of ‘pinched’ black holes, with only one of them merging with the BRs. However, these aspects are beyond the purposes of this work.)

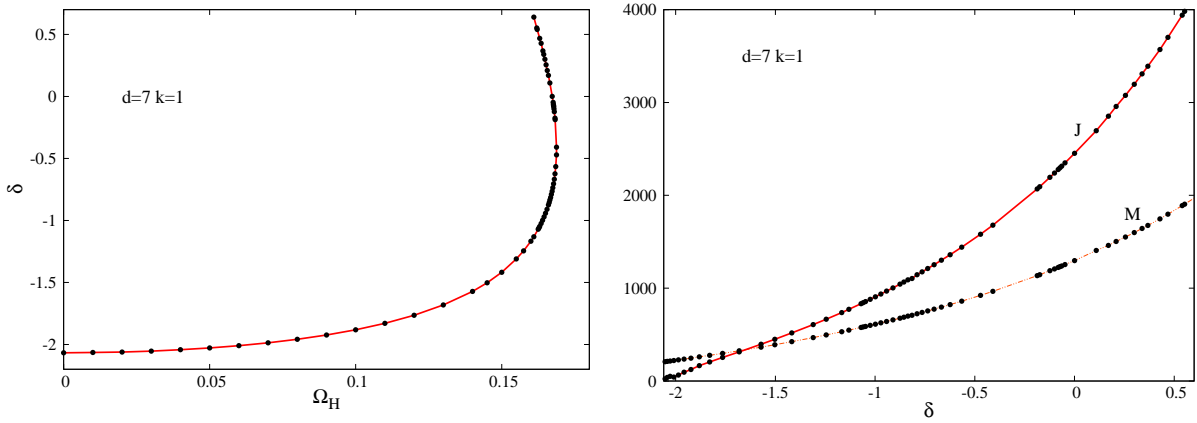


**Figure 12.** *Left:* The conical deficit/excess  $\delta$  of the (unbalanced)  $d = 7$ ,  $k = 1$  black ringoid solutions with  $r_H = 1$ ,  $R = 4.6$  is shown as a function of the angular velocity of the horizon  $\Omega_H$ . *Right:* The mass  $M$  and angular momentum  $J$  are shown *vs.*  $\delta$  for the same solutions.

In Figure 10 we show the Gibbs potential and the Helmholtz free energy of the BRs together with the corresponding MP black holes. The situation there looks rather different as compared to the  $d = 5$  case in Figure 6. This originates in the different behaviour of the MP black holes together with the existence of a critical merger solution in  $d = 6$ , with nonzero values of  $W, F$ .

Finally, in Figure 11 we exhibit the deformations of the  $S^3$  and  $S^1$ -components of the horizon, as given by the ratios  $L_e/L_p$  and  $R_1^{(in)}/R_1^{(out)}$ , as functions of the reduced angular momentum. One can see that as the critical horizon topology changing solution is approached, both  $L_e$  and  $L_p$  stay finite and nonzero. Moreover, our results suggest that this is the case as well for  $R_1^{(out)}$ , whereas  $R_1^{(in)} \rightarrow 0$ .

### 5.2.2 $k = 1$ : black ringoids in $d = 7$ dimensions

The  $d = 7$ ,  $k = 1$  solutions with a horizon topology  $S^2 \times S^3$  have very different properties from those of the  $d = 6$  BRs discussed above. This is not surprising, since the slowly rotating solutions can be described as perturbative deformations of the static configurations in [16]. The results there show that the limiting static solutions necessarily possess a conical singularity which prevents their collapse, and no other pathologies. Moreover, as discussed in [37], [38], the asymptotically flat black objects with conical singularities still admit a consistent thermodynamical description. Also, when working with the appropriate set of thermodynamical variables, the Bekenstein-Hawking law still holds for such solutions.

As expected, their (generic) rotating generalizations possess also conical singularities, while being physically acceptable in all other aspects. Moreover, this pathology has a rather neutral effect on the numerics, since the solver does not notice it directly.

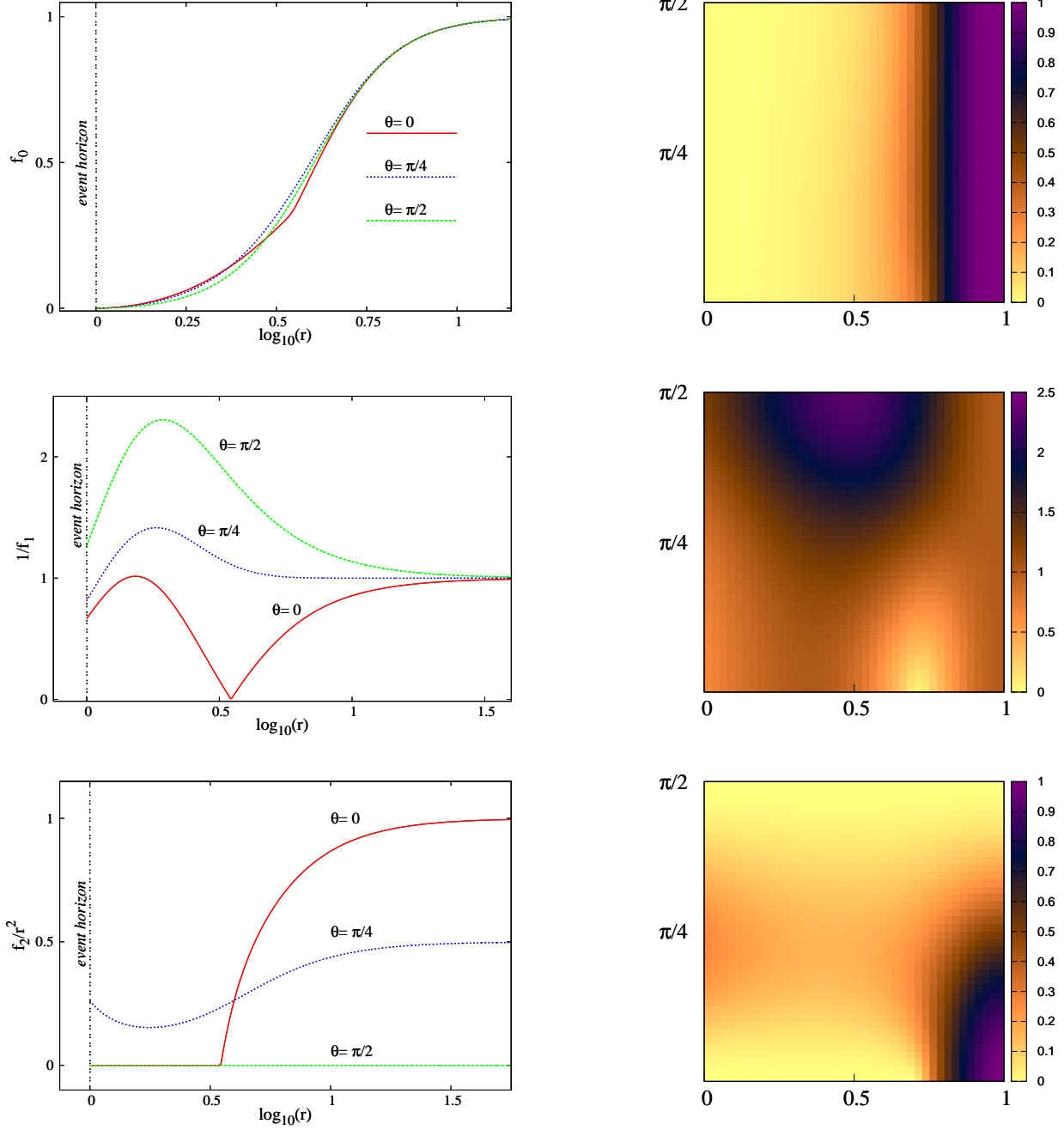


**Figure 13:** The metric functions  $f_i$ ,  $W$  and the Kretschmann scalar  $K = R_{\mu\nu\alpha\beta}R^{\mu\nu\alpha\beta}$  are shown for a  $d = 7$  black ringoid with the input parameters  $r_H = 1$ ,  $R = 3.5$  and  $\Omega_H \simeq 0.199$ .

In our work, we have chosen to locate the conical singularity at  $\theta = 0$ ,  $r_H < r < R$ , where the generic configurations have a conical deficit/excess

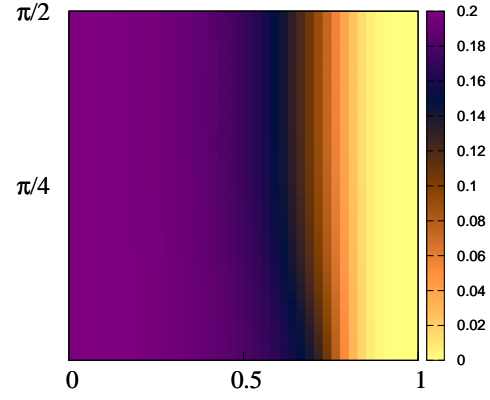
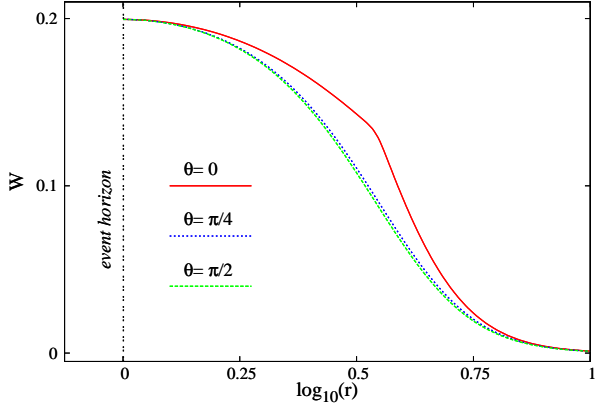
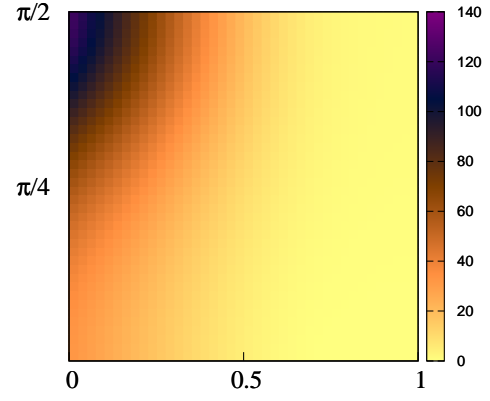
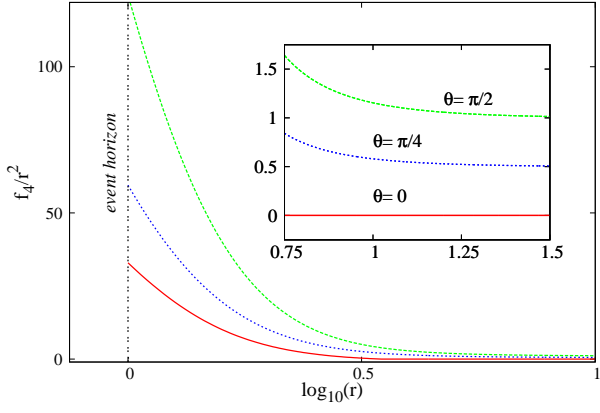
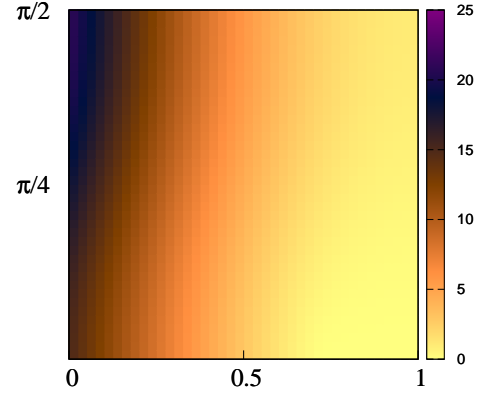
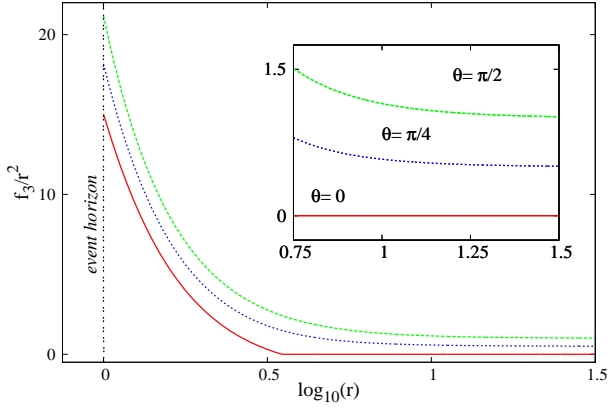


Figure 13: continued.

$$\delta = 2\pi(1 - \lim_{\theta \rightarrow 0} \frac{f_2}{\theta^2 r^2 f_1}), \quad (5.3)$$

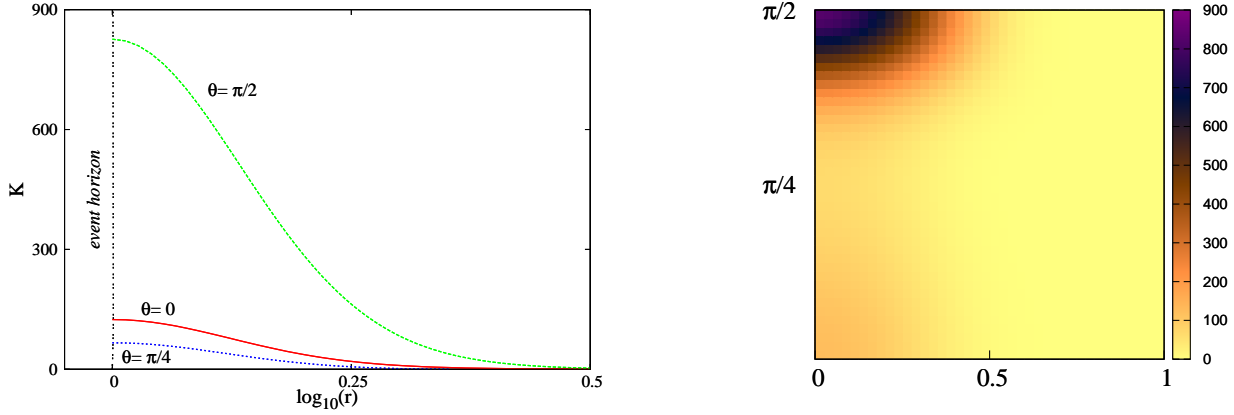


Figure 13: continued.

with  $\delta < 0$  in the static case. (Therefore these solutions satisfy the more general condition  $f_{22} = r^2 f_{10} \text{const.}$  in the  $\theta = 0$  expansion (A.11), the case  $\text{const.} = 1$  implying the absence of a conical singularity.) This can be interpreted as the higher dimensional analogue of a ‘strut’ preventing the collapse of the configurations.

As expected, adding rotation to a static solution decreases the absolute value of  $\delta$ , such that  $\delta = 0$  is realized for a critical value of  $\Omega_H$ . When the parameter  $\Omega_H$  is varied further, one finds instead an over-rotating black ringoid with a conical excess,  $\delta > 0$ .

Note also that for the solutions studied so far, the global charges increase with  $\delta$ . These features are illustrated in Figure 12, for a family of solutions with fixed  $r_H$ ,  $R$ . (Note that this behaviour is qualitatively similar to the one found for  $d = 5$  unbalanced BRs, see *e.g.* [38].)

However, a systematic study of the generic unbalanced case is beyond the purposes of this work. Therefore for the rest of this section we shall consider the physically most interesting case of balanced black ringoids.

The set of balanced solutions is constructed again by varying the parameter  $R$  for fixed  $r_H$ , looking for configurations with  $\delta = 0$ , a condition which is realized for a unique value of the input parameter  $\Omega_H$ . To the best of our knowledge, these solutions represent the first set of balanced nonperturbative solutions obtained for a non-spherical and non-ring horizon topology. We show in Figure 13 the profiles of such a typical balanced black ringoid, together with the Kretschmann scalar  $K = R_{\mu\nu\alpha\beta} R^{\mu\nu\alpha\beta}$ .

The results of the numerical integration are shown in Figure 14 for the same set of reduced quantities as in the BR case. One can see that the blackfold results provide again a very good description of the fast spinning solutions. Also, as expected, the angular momentum of the balanced black ringoids is bounded below, but not above.

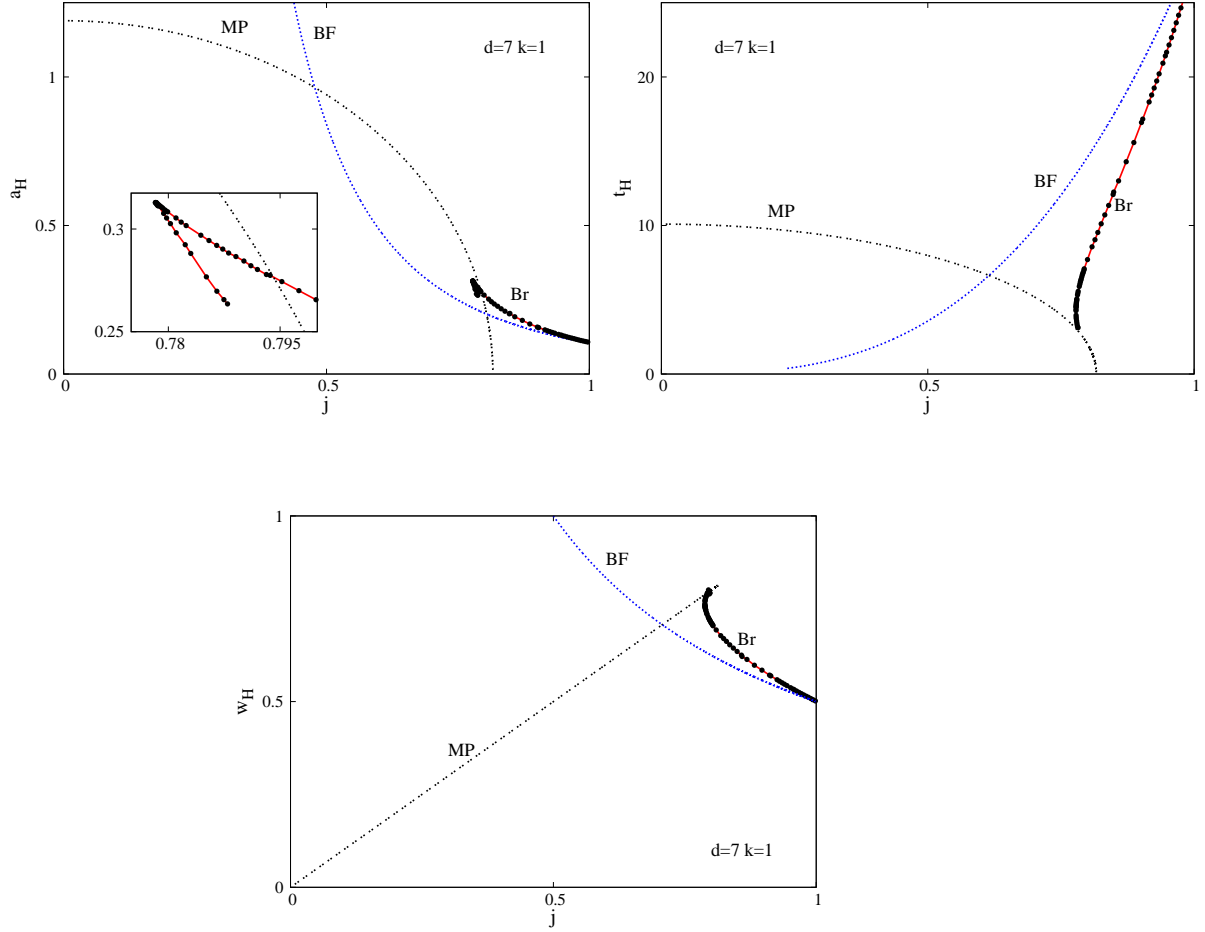


**Figure 14.** The reduced area  $a_H$ , the reduced temperature  $t_H$  and the reduced angular velocity  $w_H$  are shown *vs.* the reduced angular momentum  $j$  for  $d = 7$  black ringoids (Br) with  $S^2 \times S^3$  event horizon topology together with the corresponding results for Myers-Perry (MP) black holes with two equal angular momenta. The curves corresponding to the blackfold (BF) prediction are also shown.

Our numerical results show that, similar to BRs, there are two branches of solutions, which are dubbed again ‘thin’ and ‘fat’, according to their shape. These two branches meet in a cusp at  $j \simeq 0.778$ ,  $a_H \simeq 0.312$ , where  $a_H$  assumes its maximal value, while  $j$  takes its minimal value.

This minimally spinning solution has a non-degenerate regular horizon, and thus does not correspond to an extremal black hole. Also, for some range of  $j$ , there are three different solutions with the same global charges: one MP black hole and two black ringoids.

The numerical results strongly suggest that the branch of ‘fat’ black ringoids ends in a limiting solution with  $a_H = 0$  and a nonzero  $j$ .

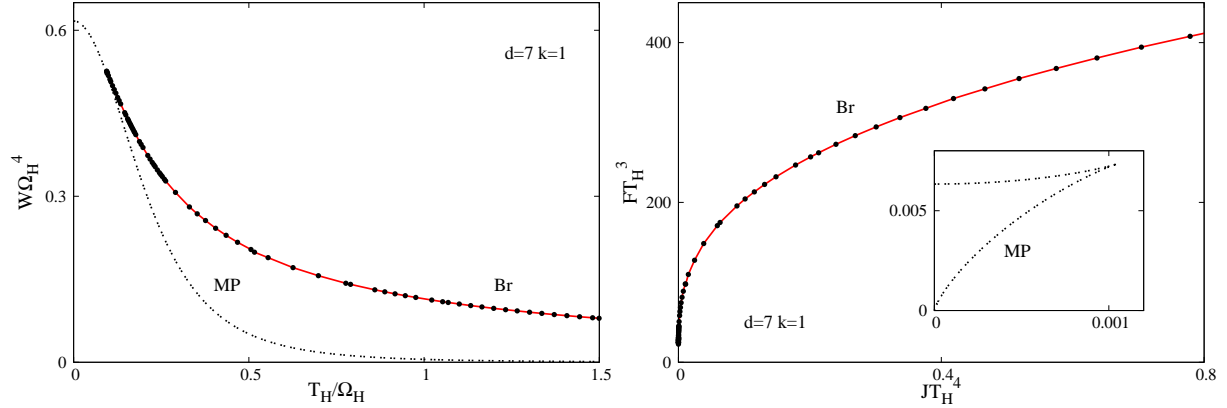


**Figure 15.** *Left:* The grand canonical potential  $W$  is shown as a function of the Hawking temperature  $T_H$  for  $d = 7$  black ringoids (Br) and Myers-Perry (MP) black holes with fixed angular velocity of the horizon  $\Omega_H$ . *Right:* The canonical potential  $F$  is shown as a function of the angular momentum  $J$  for the same  $d = 7$  solutions with fixed Hawking temperature  $T_H$ .

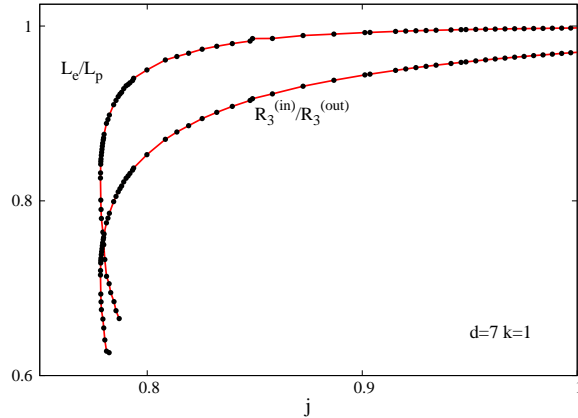


**Figure 16.** The ratios  $L_e/L_p$  and  $R_3^{(in)}/R_3^{(out)}$ , which encode the deformation of the horizon, are shown *vs.* the reduced angular momentum  $j$  for  $d = 7$ ,  $k = 1$  black ringoid solutions.

Unfortunately, the numerical accuracy deteriorates before approaching that point, so that we could not fully clarify this issue<sup>16</sup>. However, based on an extrapolation of the existing results, we conjecture that, similar to the  $d = 5$  case, this limiting solution coincides with the

<sup>16</sup>So far, we did not manage to construct solutions for  $R/r_H < 1.7$  with good accuracy, obtaining large errors (in particular, for the constraint equations) for smaller values of this ratio. However, we believe that this is a numerical problem only. We conjecture that the numerical difficulties we encounter are related to the singular nature of the  $R \rightarrow r_H$  limiting solution. For example, an analysis of the  $d = 5$  BR solution in Appendix B shows that some metric functions (as well as some global quantities) diverge in this limit.

extremal MP black hole, forming a naked singularity.

A further argument that this is indeed the case is suggested by the results in [16]. There the  $d = 7$  static solutions with  $S^2 \times S^3$  horizon topology have been constructed in a systematic way (although in a different coordinate system, see also [17]). The results there indicate that as  $R/r_H \rightarrow 1$ , the black ringoids approach a solution with  $S^5$  horizon topology (*i.e.* the Schwarzschild-Tangerlini black hole). Thus it is natural to expect that this continues to hold when these configurations are spinning.

Moreover, this is also suggested by the plots of the thermodynamical potentials in Figure 15, which resemble again the  $d = 5$  case. Also the ratios  $L_e/L_p$  and  $R_3^{(in)}/R_3^{(out)}$ , which encode the deformation of the horizon (see Figure 16), follow the pattern of Figure 7, although our last reliable numerical results are still far away from the putative limiting solution with  $L_p \rightarrow \infty$ ,  $R_1^{(in)} \rightarrow 0$ .

### 5.2.3 Further cases and the conjectured picture

Let us start with the case of BRs in  $d = 7$ . So far, we have constructed only solutions on the branch of thin BRs. (We mention that our approach here was similar to the  $d = 6$  case. In particular, the generic solutions found were again singular, with singularities stronger than the conical ones.) However, the recent results in [20] (see also [39]) clearly show that the picture found for the nonperturbative region in  $d = 6$  holds also in  $d = 7$ . Again there exist two branches of solutions; the branch of ‘fat’ black rings connects via a topology-changing merger solution with a branch of ‘pinched’ black hole solutions. In particular, the diagrams for the reduced physical properties look very similar to those in Figure 9. We expect that this picture remains valid for BR solutions in  $d > 7$  dimensions as well.

Returning to the case of black ringoids (*i.e.*  $k > 0$ ), we mention that we have managed to construct a number of solutions for  $d = 8$  and  $d = 9$ , possessing  $S^3 \times S^3$  and  $S^2 \times S^5$  horizon topologies, respectively. However, although we could confirm their existence, we have not yet managed to study their properties in a systematic way. All configurations we could obtain so far are well described by the blackfold results. But the numerical accuracy decreases and the solutions are lost well before approaching the respective branches of ‘fat’ black ringoids. We believe that a refinement of the numerical scheme is required in order to succeed in obtaining those branches.

Let us mention that the properties of the generic (unbalanced) solutions are different for  $d = 8$  as compared to  $d = 9$ . The numerical construction of the  $d = 8$  black ringoids with  $S^3 \times S^3$  horizon topology is similar to the one of the  $d > 5$  BRs. In particular, all generic configurations appear to be singular and a ‘shooting’ procedure is required in order to construct regular solutions (analogous to the  $d > 5$  BRs discussed above). Also, since there is no upper bound on the angular momenta for the corresponding  $n = 2$ ,  $k = 1$  MP black holes, we expect the existence of new branches of axisymmetric ‘pinched’ black holes with a spherical horizon topology. These black holes would branch off from the MP solutions along the stationary axisymmetric zero-mode perturbation of the Gregory-Laflamme-like instability.



As suggested by the  $k = 0$  pattern observed for  $d = (6, 7)$  BRs, we expect the ‘pinched’ black holes to connect these  $d = 8$  black ringoids with the MP black holes.

By contrast, the generic  $d = 9$  configurations with  $S^2 \times S^5$  horizon topology are supported against collapse by conical singularities, their (well-defined) static limit being considered in [16], in a more general context. Similar to the  $d = 7$  black ringoids discussed above, the balanced configurations are found by finetuning the value of the event horizon velocity  $\Omega_H$  for given input parameters  $(r_H, R)$ . Since the angular momentum of the corresponding  $n = 1$ ,  $k = 2$  MP solutions is bounded from above, no branches of ‘pinched’ black holes are expected to exist in this case. Therefore we conjecture the picture found for  $d = 5$  black objects to be valid also for these configurations, the  $n = 1$ ,  $k = 2$  black ringoids and MP black holes meeting in a nakedly singular configuration given by (4.9).

## 6. Conclusions and further remarks

The last decade has witnessed a tremendous progress in the physics of black objects with a non-spherical horizon topology. These developments, originating in the discovery by Emparan and Reall of the  $d = 5$  BR, have revealed the existence of a zoo of higher dimensional solutions with various topologies of the event horizon. However, while the ultraspinning regime of some of these objects is very well described by the corresponding blackfolds, the behaviour of the solutions in other regions of the parameter space is relatively poor understood. In particular, only little is known about their limiting behaviour and topology-changing mergers with branches of ‘pinched’ black holes, emerging from the respective known MP black hole solutions.

In the absence of analytical solutions, one possible approach to make progress in this direction is to solve the Einstein equations numerically. In this work, by using a special coordinate system, we have been able to formulate the problem of (a class of)  $d \geq 5$  balanced black objects with  $S^{n+1} \times S^{2k+1}$  event horizon topology in a numerically manageable manner. Thus such solutions can be constructed numerically, by solving a set of elliptic partial differential equations (with a dependence on two variables only), with suitable boundary conditions. These boundary conditions enforce the topology of the horizon and the asymptotic structure of the spacetime.

A number of nonperturbative solutions have been constructed in this way. Our results for  $d = 6$  BRs have confirmed the conjecture of [10] for the phase diagram of such objects. In particular, the limiting behaviour of the ‘fat’ black ring solutions is very different as compared to the  $d = 5$  case, since they are connected to the MP black hole via a set of ‘pinched’ black holes. We have found a different picture for  $d = 7$  black ringoids with two equal angular momenta. Although we could not fully explore this case, a number of features (observed in the phase diagrams for the physical properties and the thermodynamics) strongly suggest that these configurations share the properties of the  $d = 5$  BRs. In particular, they are likely to meet the corresponding MP black holes in a limiting (nakedly singular) extremal configuration.

Another interesting new result is the occurrence of a cusp in the  $a_H(j)$  black ring(oid) diagram, where a branch of ‘fat’ black ring(oid) solutions emerges. Since this is the case for all known solutions, we expect this to hold generically. Thus nonuniqueness with respect to the global charges also appears to be a generic property of these solutions.

As possible avenues for future research, let us mention that the general ansatz in Section 3 as well as the specific solutions in Section 5 can be extended to study black objects possessing an  $S^{n+1} \times S^{2k+1}$  horizon topology, with rotation not only on the  $S^{2k+1}$  but also on the  $S^{n+1}$ . However, in this case,  $n$  should be an odd number,  $n = 2p + 1$ , and the angular momenta in that sector should all be equal as well (although their magnitude could differ from the one of the angular momenta on the  $S^{2k+1}$ ). This extension would involve more functions in the metric ansatz, but no new conceptual difficulty should arise, the problem remaining of codimension-two. Moreover, our methods should readily extend to more general situations, *e.g.* to the presence of matter fields [40], [19], or for anti-de Sitter asymptotics of the spacetime background. The latter case is of special interest, given the absence of exact solutions even for  $d = 5$  (see, however, [41], [42] for results found within the blackfold approach). Also, it should be interesting to consider multi-black hole configurations and to extend the phase diagram proposed in [43] to the fully nonperturbative regime.

Finally, let us speculate about another possible implication of the results in this work. Hopefully, the activity in the area of higher dimensional black objects will result in an encyclopedia of solutions, with a well-understood phase space. Then we consider it very likely that, at some stage, some general structures would be revealed, leading to a description of the solutions in terms of a number of (relatively) simple patterns. Let us exemplify this with the case of the particular classes of MP black holes and the  $S^{n+1} \times S^{2k+1}$  black ring(oid)s in this work. We expect that the well-known picture found for  $d = 5$ ,  $k = 0$  is generic for all higher dimensional solutions with  $n = 1$ , *i.e.* for black ringoids with  $S^2 \times S^{d-4}$  event horizon topology and the corresponding MP black holes with  $k + 1$  equal angular momenta in  $d = 2k + 5$  dimensions. Thus we conjecture that the diagrams in Figures 5-7 should always apply for these  $n = 1$  solutions, with the branch of ‘fat’ black ringoids meeting the MP solutions in the zero-area configuration (4.9). At the same time, we expect the properties of the known  $d = 6, 7$  BRs (in conjunction with the corresponding MP and ‘pinched’ black holes) to provide the pattern for all balanced black objects with  $S^{n+1} \times S^{2k+1}$  horizon topology and with  $n > 1$ . Moreover, it is likely that more complicated black objects will exhibit a generic behaviour as well (*e.g.* the  $d = 5$  doubly spinning BRs [44] would provide the pattern for  $S^2 \times S^{2k+1}$  black ringoids with un-equal angular momenta, possibly spinning also on the  $S^2$ ).

Such a classification should result at some stage in a *periodic table* of higher dimensional black objects, organized on the basis of a small number of characteristic features.

**Acknowledgements.**— We would like to thank C. Herdeiro, N. Obers and J. Rocha for helpful discussions at various stages of this project. We acknowledge support by the DFG Research Training Group 1620 Models of Gravity. E.R. acknowledges support from the

FCT-IF programme.

## A. The approximate form of the solutions on the boundaries

In our work, we have found it useful to construct an approximate form of the solutions on the boundaries of the domain of integration. There we suppose the existence of a power series expansion at the horizon/infinity and also at  $\theta = 0, \pi/2$ . Also, we assume that the metric functions  $f_i$  ( $i = 1, 4$ ) preserve the behaviour on the boundaries of the background metric. Here we recall that for black objects with an  $S^{n+1} \times S^{2k+1}$  horizon topology, the relevant part of the background metric is given by (2.15). At the same time, the obvious background for black holes with a spherical horizon topology is (2.1).

### A.1 The horizon

As  $r \rightarrow r_H$ , it is natural to suppose that the non-extremal solutions (which are the only type constructed in this work), possess a power series expansion of the form (here we assume a metric gauge with  $\Delta(r) = r^2$ ; also, the relations below hold as well for a spherical topology of the horizon):

$$f_i(r, \theta) = \sum_{j \geq 0} f_{ij}(\theta)(r - r_H)^j, \quad W(r, \theta) = \sum_{j \geq 1} w_j(\theta)(r - r_H)^j, \quad (\text{A.1})$$

with nonvanishing  $f_{10}, f_{20}, f_{30}, f_{40}$  and a double zero for  $f_0$ ,

$$f_0(r, \theta) = f_{02}(r - r_H)^2 + \sum_{j \geq 3} f_{ij}(\theta)(r - r_H)^j. \quad (\text{A.2})$$

Then the Einstein equations are solved order by order in  $\epsilon = (r - r_H)$ , which lead to a solution in terms of five functions

$$\{f_{02}(\theta), f_{20}(\theta), f_{30}(\theta), f_{40}(\theta), w_2(\theta)\}, \quad (\text{A.3})$$

and two constants

$$\{c_1 = \frac{f_{10}(\theta)}{f_{02}(\theta)}, \quad w_0 = \Omega_H\}, \quad (\text{A.4})$$

which fix the Hawking temperature and the event horizon velocity of the black objects.

We have verified that, at least up to order six, all other functions in (A.1) vanish or are fixed by (A.3), (A.4). For example, one finds

$$f_{21} = f_{31} = f_{41} = w_1 = 0, \quad f_{03} = -\frac{f_{02}}{r_H}, \quad f_{11} = -\frac{2f_{10}}{r_H}, \quad w_3 = -\frac{w_2}{r_H}, \quad (\text{A.5})$$

while

$$f_{04} = \frac{1}{12} \left( \frac{11f_{02}}{r_H^2} - \frac{4f_{02}f_{32}}{f_{30}} - \frac{8kf_{02}f_{42}}{f_{40}} + 8f_{30}w_2^2 + \frac{\dot{f}_{02}^2}{r_H^2 f_{02}} \right. \\ \left. - \frac{(d-2k-4)}{f_{20}} (4f_{02}f_{22} + \frac{\dot{f}_{02}\dot{f}_{20}}{r_H^2}) - \frac{\dot{f}_{02}\dot{f}_{30}}{r_H^2 f_{30}} - \frac{2k\dot{f}_{02}\dot{f}_{40}}{r_H^2 f_{40}} - \frac{2\ddot{f}_{02}}{r_H^2} \right). \quad (\text{A.6})$$

In a numerical approach, the functions (A.3) together with the constant  $c_1$  are read from the numerical output.

For completeness, we give also the approximate form of the metric close to the horizon

$$ds^2 = f_{02}(\theta)(c_1(dr^2 + r_H^2 d\theta^2) - (r - r_H)^2 dt^2) + f_{20}(\theta)d\Omega_n^2 + f_{30}(\theta)(d\psi + \mathcal{A} - \Omega_H dt)^2 + f_{40}(\theta)d\Sigma_k^2. \quad (\text{A.7})$$

## A.2 The $\theta = 0$ boundary

The situation is more complicated in this case, since the black holes with  $S^{n+1} \times S^{2k+1}$  horizon topology, possess a different expansion for  $r_H \leq r < R$  and for  $r > R$ , respectively. (This feature can be understood from the study in Section 2 of background functions  $F_i$ .)

For  $r_H \leq r < R$  and  $\theta \rightarrow 0$ , the solutions with a non-spherical horizon topology can be written as

$$f_i(r, \theta) = \sum_{j \geq 0} f_{ij}(r)\theta^j, \quad W(r, \theta) = \sum_{j \geq 0} w_j(r)\theta^j, \quad (\text{A.8})$$

with

$$f_2(r, \theta) = f_{22}(r)\theta^2 + \sum_{j \geq 3} f_{2j}(r)\theta^j. \quad (\text{A.9})$$

The essential functions in this expansion are

$$\{f_{00}(r), f_{10}(r), f_{30}(r), f_{40}(r), w_0(r)\}, \quad (\text{A.10})$$

all other functions in (A.8) vanishing or being fixed by those in (A.10). One finds *e.g.*

$$f_{01} = f_{11} = f_{31} = f_{41} = f_{23} = w_1 = 0, \quad f_{22} = r^2 f_{10}, \quad (\text{A.11})$$

and

$$f_{42} = \frac{r^2}{4(d-2k-3)} \left( 8f_{10} \left( 1 + k - \frac{f_{30}}{f_{40}} \right) - \left( \frac{2(d-2k-3)}{r} + \frac{f'_{00}}{f_{00}} + \frac{(d-2k-4)f'_{10}}{f_{10}} + \frac{f'_{20}}{f_{30}} \right) f'_{40} - \frac{2(k-1)}{f_{40}} f_{40}'' - 2f_{40}'' \right). \quad (\text{A.12})$$

Therefore for  $r_H < r < R$ , the approximate form of the line element close to  $\theta = 0$  reads

$$ds^2 = f_{10}(r) (dr^2 + r^2(d\theta^2 + \theta^2 d\Omega_n^2)) - f_{00}(r)dt^2 + f_{30}(r)(d\psi + \mathcal{A} - w_0(r)dt)^2 + f_{40}(r)d\Sigma_k^2. \quad (\text{A.13})$$

An expansion similar to (A.8) holds also for  $r > R$ , with

$$f_3(r, \theta) = f_{32}(r)\theta^2 + \sum_{j \geq 3} f_{3j}(r)\theta^j, \quad f_4(r, \theta) = f_{42}(r)\theta^2 + \sum_{j \geq 3} f_{4j}(r)\theta^j, \quad (\text{A.14})$$

and (with  $i = 1, 2$ )

$$f_i(r, \theta) = \sum_{j \geq 0} f_{ij}(r) \theta^j, \quad W(r, \theta) = \sum_{j \geq 0} w_j(r) \theta^j, \quad (\text{A.15})$$

in this case. The essential functions here are

$$\{f_{00}(r), f_{10}(r), f_{20}(r), w_0(r)\}, \quad (\text{A.16})$$

while, *e.g.*

$$f_{01} = f_{11} = f_{21} = f_{33} = f_{43} = w_1 = 0, \quad f_{32} = f_{42} = r^2 f_{10}, \quad (\text{A.17})$$

such that the approximate form of the line element close to  $\theta = 0$  and  $r > R$  reads

$$ds^2 = f_{10}(r) \left( dr^2 + r^2 [d\theta^2 + \theta^2 ((d\psi + \mathcal{A} - w_0(r)dt)^2 + d\Sigma_k^2)] \right) + f_{20}(r) d\Omega_n^2 - f_{00}(r) dt^2.$$

For black holes with a spherical horizon topology, one can formally take  $R = r_H$ , such that the relations (A.14)-(A.18) hold in that case for any  $r > r_H$ .

### A.3 The $\theta = \pi/2$ boundary

The corresponding expansion as  $\theta \rightarrow \pi/2$  reads

$$f_i(r, \theta) = \sum_{j \geq 0} f_{ij}(r) (\theta - \frac{\pi}{2})^j, \quad W(r, \theta) = \sum_{j \geq 0} w_j(r) (\theta - \frac{\pi}{2})^j, \quad (\text{A.18})$$

with

$$f_2(r, \theta) = f_{22}(r) (\theta - \frac{\pi}{2})^2 + \sum_{j \geq 3} f_{2j}(r) (\theta - \frac{\pi}{2})^j, \quad (\text{A.19})$$

the essential functions in this expansion being

$$\{f_{00}(r), f_{10}(r), f_{30}(r), f_{40}(r), w_0(r)\}, \quad (\text{A.20})$$

all other functions in (A.8) vanishing or being fixed by (A.20). Note that the relations (A.11), (A.12) still hold in this case (although the corresponding expressions of the functions are different, of course). Then the approximate form of the line element close to  $\theta = \pi/2$  reads

$$ds^2 = f_{10}(r) \left( dr^2 + r^2 (d\theta^2 + (\theta - \frac{\pi}{2})^2 d\Omega_n^2) \right) - f_{00}(r) dt^2 + f_{30}(r) (d\psi + \mathcal{A} - w_0(r)dt)^2 + f_{40}(r) d\Sigma_k^2. \quad (\text{A.21})$$

The above relations hold for both a  $S^{d-2}$  and  $S^{n+1} \times S^{2k+1}$  horizon topology.

#### A.4 The expansion as $r \rightarrow \infty$

Finally, the solutions admit a  $1/r$  expansion as  $r \rightarrow \infty$ , with

$$\begin{aligned} f_1(r, \theta) &= 1 + \sum_{j \geq 2} \frac{f_{1j}(\theta)}{r^j}, \quad f_2(r, \theta) = r^2 \cos^2 \theta \left(1 + \sum_{j \geq 2} \frac{f_{2j}(\theta)}{r^j}\right), \\ f_3(r, \theta) &= r^2 \sin^2 \theta \left(1 + \sum_{j \geq 2} \frac{f_{3j}(\theta)}{r^j}\right), \quad f_4(r, \theta) = r^2 \sin^2 \theta \left(1 + \sum_{j \geq 2} \frac{f_{4j}(\theta)}{r^j}\right), \\ f_0(r, \theta) &= 1 + \sum_{j \geq d-3} \frac{f_{0j}(\theta)}{r^j}, \quad W(r, \theta) = \sum_{j \geq d-1} \frac{w_j(\theta)}{r^j}, \end{aligned} \quad (\text{A.22})$$

with

$$f_{0(d-3)} = C_t, \quad w_{d-1} = C_\psi \quad (\text{A.23})$$

two constants which fix the mass and angular momentum, respectively.

#### A.5 On the regularity of the solutions

One can easily verify that the MP black holes and the  $d = 5$  Emparan-Reall black ring are regular on and outside the event horizon. However, given their numerical character, this is not obvious for the other solutions discussed in this work. In particular, the numerical scheme employed in this work uses a special coordinate system which implies the existence of a singularity at  $(r = R, \theta = 0)$ . This singularity is already present for the  $D = 4$  flat space case discussed in Section 2. However, one can show that similar to that case, the point  $(r = R, \theta = 0)$  is just a coordinate singularity, assuming that the metric functions satisfy the  $\theta \rightarrow 0$  expansion discussed above.

To prove that, we recall first that within our numerical scheme the functions  $f_i$  ( $i > 0$ ) which enter the general line element (3.1) are taken as

$$f_i = F_i \mathcal{F}_i, \quad i = 1, 2, 3, \quad \text{and} \quad f_4 = F_3 \mathcal{F}_4, \quad (\text{A.24})$$

with  $(F_1, F_2, F_3)$  given by (2.12), and the unknown functions  $\mathcal{F}_1, \mathcal{F}_2, \mathcal{F}_3, \mathcal{F}_4$  which are found numerically.

Next, in order to focus on the region around the point  $(r = R, \theta = 0)$ , we change to adapted coordinates

$$r \sin \theta = \frac{1}{2R\mathcal{F}_1(R, 0)} \rho^2 \sin 2\Theta, \quad r \cos \theta = R + \frac{1}{2R\mathcal{F}_1(R, 0)} \rho^2 \cos 2\Theta, \quad (\text{A.25})$$

such that  $(r = R, \theta = 0)$  now lies at  $\rho = 0$ , and then expand the metric in powers of  $\rho$ . To leading order terms in  $\rho^2$ , the expression of the line element is

$$\begin{aligned} ds^2 &= d\rho^2 + \rho^2 d\Theta^2 + \frac{\mathcal{F}_2(R, 0)}{\mathcal{F}_1(R, 0)} \rho^2 \cos^2 \Theta d\Omega_n^2 - f_0(R, 0) dt^2 \\ &\quad + \frac{\mathcal{F}_3(R, 0)}{\mathcal{F}_1(R, 0)} \rho^2 \sin^2 \Theta (d\psi + \mathcal{A} - W(R, 0) dt)^2 + \frac{\mathcal{F}_4(R, 0)}{\mathcal{F}_1(R, 0)} \rho^2 \sin^2 \Theta d\Sigma_k^2. \end{aligned} \quad (\text{A.26})$$

However, one can easily see that the approximate solution constructed in Appendix A2 implies<sup>17</sup>  $\mathcal{F}_3(R, 0) = \mathcal{F}_4(R, 0) = \mathcal{F}_1(R, 0)$ . As a result, (A.26) is just the flat spacetime metric written in the form (2.1), (2.2). Thus we conclude that the point  $(r = R, \theta = 0)$  is a coordinate singularity only.

To further investigate the regularity of the numerical solutions, we have analyzed both analytically and numerically their Kretschmann scalar<sup>18</sup>

$$K = R_{\mu\nu\alpha\beta}R^{\mu\nu\alpha\beta}. \quad (\text{A.27})$$

Unfortunately, we have not been able to find a general expression for  $K$  valid for any  $(d, k)$ , similar to that found for the Einstein tensor. Therefore we have restricted our analytical study to a set of  $(d, k)$ . However, for all considered cases, we have found that the Kretschmann scalar is finite on the boundary of the domain of integration, for generic solutions possessing the approximate form discussed above<sup>19</sup>.

We have also investigated the expression of the Kretschmann scalar, as resulting from the numerical integration of the Einstein equations, for a number of  $d = 6$  black rings and  $d = 7$  black ringoids. As seen in Figures 8, 13, the scalar  $K$  is finite everywhere and approaches its maximal value on the horizon at  $\theta = \pi/2$  (a similar behaviour can be noticed for the considered  $d = 5$  Emparan-Reall black ring and also for the  $d = 7$  MP black hole, see Figures 4, 3). One can see also the absence of any special features at  $(r = R, \theta = 0)$ , the Kretschmann scalar being always finite there.

## B. Five-dimensional black rings

### B.1 The solution

The expression of the metric functions which enter the line element (4.10) reads<sup>20</sup>

$$\begin{aligned} f_0(r, \theta) &= \frac{Q_2(r, \theta)}{Q_1(r, \theta)} U_1(r, \theta) U_2(r, \theta), \quad f_1(r, \theta) = \frac{r_H^2 R^4}{(R^4 - r_H^4)^2} \frac{U_1(r, \theta) Q_3(r, \theta)}{S(r, \theta)}, \\ f_2(r, \theta) &= \left(1 + \frac{r_H^2}{r^2}\right)^2 \frac{r^2 \sin^2 2\theta}{2U_2(r, \theta)}, \quad f_3(r, \theta) = \frac{r^2 \left(1 - \frac{r_H^2}{r^2}\right)^2}{2 \left(1 + \frac{r_H^2}{r^2}\right)^2} \frac{Q_1(r, \theta)}{Q_2(r, \theta) U_1(r, \theta)}, \\ W(r, \theta) &= \frac{4\sqrt{2}(r_H^2 + R^2) \sqrt{R^4 + r_H^4}}{R(R^2 - r_H^2)} \frac{\left(1 - \frac{r_H^2}{r^2}\right)^2}{r^2 \left(1 + \frac{r_H^2}{r^2}\right)^2} \frac{Q_2(r, \theta) Q_4(r, \theta)}{Q_1(r, \theta)}. \end{aligned} \quad (\text{B.1})$$

---

<sup>17</sup>This follows from the last relations in (A.11), (A.17) together with the expression (2.12) of the functions  $F_i$ .

<sup>18</sup>Note that a finite Kretschmann scalar does not exclude the existence of other, more subtle pathologies, see *e.g.* [45] for a recent example in this direction.

<sup>19</sup>Here we assume that the various functions  $f_{ij}$ ,  $W_i$  which enter the approximate solution on the boundaries are finite, together with their first and second derivatives.

<sup>20</sup>A slightly more complicated form of these functions has been given in [17].

In the above relations, we have defined a number of auxiliary functions

$$\begin{aligned} U_1(r, \theta) &= \frac{(r_H^2 + R^4)}{r_H^2 R^2} \left( 1 + \frac{4r_H^2}{r^2} + \frac{r_H^4}{r^4} \right) + \frac{4r_H^2}{r^2} \cos 2\theta - 2S(r, \theta), \\ U_2(r, \theta) &= \frac{r_H^2 + R^4}{r^2 R^2} - \left( 1 + \frac{r_H^4}{r^4} \right) \cos 2\theta + S(r, \theta), \end{aligned} \quad (\text{B.2})$$

together with

$$\begin{aligned} Q_1(r, \theta) &= U_1^2(r, \theta) U_2(r, \theta) - \frac{4(r_H^2 + R^2)^2 (r_H^4 + R^4)}{r^2 R^2 (R^2 - r_H^2)^2} \frac{\left( 1 + \frac{r_H^2}{r^2} \right)^2}{\left( 1 - \frac{r_H^2}{r^2} \right)^2} \times \\ &\quad \left[ U_1(r, \theta) - \left( \frac{(r_H^2 - R^2)^2}{r_H^2 R^2} + \frac{r_H^2 (r_H^2 - R^2)^2}{r^4 R^2} + \frac{2(r_H^2 + R^2)^2}{r^2 R^2} + \frac{4(r_H^4 + R^4)}{r^2 R^2} \right) \right]^2, \\ Q_2(r, \theta) &= U_1(r, \theta) - \frac{8(r_H^4 + R^4)}{r^2 R^2}, \\ Q_3(r, \theta) &= -U_1(r, \theta) + \left( 1 + \frac{r_H^2}{r^2} \right)^2 \frac{2(r_H^4 + R^4)}{r_H^2 R^2}, \\ Q_4(r, \theta) &= U_2(r, \theta) - 2 \left( 1 - \frac{r_H^2}{r^2} \right)^2 \sin^2 \theta, \end{aligned}$$

where

$$S(r, \theta) = \sqrt{\left( 1 + \frac{R^4}{r^4} - \frac{2R^2}{r^2} \cos 2\theta \right) \left( 1 + \frac{r_H^8}{r^4 R^4} - \frac{2r_H^4}{r^2 R^2} \cos 2\theta \right)}. \quad (\text{B.3})$$

## B.2 The expansion of the metric functions on the boundaries

To make contact with the generic expressions in Appendix A, it is useful to give the form of these metric functions on the boundaries of the domain of integration. Thus, for  $r \rightarrow \infty$  one finds

$$\begin{aligned} f_0(r, \theta) &= 1 - \frac{8r_H^2 (R^4 + r_H^4)}{(R^2 - r_H^2)^2} \frac{1}{r^2} + O(1/r^4), \\ f_1(r, \theta) &= 1 + \frac{1}{R^2 (R^2 - r_H^2)^2} \left( 4R^2 r_H^2 (R^4 + r_H^4) + ((R^4 + r_H^4)^2 \right. \\ &\quad \left. - 2R^2 r_H^2 (R^2 - r_H^2)^2 + 4R^4 r_H^4) \cos 2\theta \right) \frac{1}{r^2} + O(1/r^4), \\ f_2(r, \theta) &= r^2 \cos^2 \theta \left( 1 - \frac{(R^2 - r_H^2)^2 - 2R^2 r_H^2}{R^2} \right) + O(1/r^2), \\ f_3(r, \theta) &= r^2 \sin^2 \theta \left( 1 + \frac{(R^4 + r_H^4)^2 + 2R^2 r_H^2 ((R^2 + r_H^2)^2 + 2R^2 r_H^2)}{R^2 (R^2 - r_H^2)^2} \right) + O(1/r^2), \\ W(r, \theta) &= \frac{4\sqrt{2} r_H^2 (R^2 + r_H^2)^3 \sqrt{R^4 + r_H^4}}{R (R^2 - r_H^2)^3} \frac{1}{r^4} + O(1/r^6). \end{aligned} \quad (\text{B.4})$$



The corresponding expression close to the horizon,  $r = r_H$  is

$$\begin{aligned}
f_0(r, \theta) &= \frac{(R^2 - r_H^2)^2(R^4 + r_H^4 + 2R^2r_H^2 \cos 2\theta)}{2r_H^2(R^2 + r_H^2)^2(R^4 + r_H^4)}(r - r_H)^2 + O(r - r_H)^4, \\
f_1(r, \theta) &= \frac{16R^2r_H^2(R^4 + r_H^4 + 2R^2r_H^2 \cos 2\theta)}{(R^4 - r_H^4)^2} + O(r - r_H), \\
f_2(r, \theta) &= \frac{4R^2r_H^4 \sin^2 2\theta}{R^4 + r_H^4 - 2R^2r_H^2 \cos 2\theta} + O(r - r_H)^2, \\
f_3(r, \theta) &= \frac{2(R^2 + r_H^2)(R^4 + r_H^4)}{R^2(R^2 - r_H^2)^2} \frac{(R^4 + r_H^4 - 2R^2r_H^2 \cos 2\theta)}{(R^4 + r_H^4 + 2R^2r_H^2 \cos 2\theta)} + O(r - r_H)^2, \\
W(r, \theta) &= \frac{R(R^2 - r_H^2)}{\sqrt{2}(R^2 + r_H^2)\sqrt{R^4 + r_H^4}} + O(r - r_H)^2.
\end{aligned} \tag{B.5}$$

The expansion at  $\theta = 0$  for  $r_H \leq r < R$  reads:

$$\begin{aligned}
f_0(r, \theta) &= \frac{(r^2 - r_H^2)^2(R^2 - r_H^2)^2}{r^4(R^2 - r_H^2)^2 + r_H^4(R^2 - r_H^2)^2 + 2r^2r_H^2(3R^4 + 2R^2r_H^2 + 3r_H^4)} + O(\theta)^2, \\
f_1(r, \theta) &= \frac{(r^2 + r_H^2)^4}{r^8 \left( \frac{R^4 + r_H^4}{r^2 R^2} - \frac{r_H^4}{r^4} - 1 \right)} + O(\theta)^2, \\
f_2(r, \theta) &= \frac{R^2(r^2 + r_H^2)^4}{r^4(R^4 + r_H^4) - r^2R^2r_H^4 - r^6R^2} \theta^2 + O(\theta)^4, \\
f_3(r, \theta) &= \left( r^2(R^4 + r_H^4) - R^2r_H^4 - r^4R^2 \right) \left( r^4(R^2 - r_H^2)^2 + r_H^4(R^2 - r_H^2)^2 \right. \\
&\quad \left. + 2r^2r_H^2(3R^4 + 2R^2r_H^2 + 3r_H^4) \right) \frac{1}{r^2R^2(r^2 + r_H^2)^2(R^2 - r_H^2)^2} + O(\theta)^2, \\
W(r, \theta) &= \frac{4\sqrt{2}r^2Rr_H^2(R^2 - r_H^2)\sqrt{R^4 + r_H^4}}{(R^2 + r_H^2) \left( r^4(R^2 - r_H^2)^2 + r_H^4(R^2 - r_H^2)^2 + 3r^2r_H^2(3R^4 + 2R^2r_H^2 + 3r_H^4) \right)} + O(\theta)^2.
\end{aligned} \tag{B.6}$$

A different expansion holds at  $\theta = 0$  for  $r \geq R$ :

$$\begin{aligned}
f_0(r, \theta) &= \frac{(r^2 - r_H^2)^2(R^2 - r_H^2)^2}{r^4(R^2 - r_H^2)^2 + r_H^4(R^2 - r_H^2)^2 + 2r^2r_H^2(3R^4 + 2R^2r_H^2 + 3r_H^4)} + O(\theta)^2, \\
f_1(r, \theta) &= \frac{R^2(r^2 - r_H^2)^2((r^4 + r_H^4)(R^2 - r_H^2)^2 + 2r^2r_H^2(3R^4 + 2R^2r_H^2 + 3r_H^4))}{r^4(R^2 - r_H^2)^2(R^2(r^4 + r_H^4) - r^2(R^4 + r_H^4))} + O(\theta)^2, \\
f_2(r, \theta) &= \frac{(r^2 + r_H^2)^2(R^2(r^4 + r_H^4) - r^2(R^4 + r_H^4))}{r^2R^2(r^2 - r_H^2)^2} + O(\theta)^2, \\
f_3(r, \theta) &= \frac{R^2(r^2 - r_H^2)^2((R^2 - r_H^2)^2(r^4 + r_H^4) + 2r^2r_H^2(3R^4 + 2R^2r_H^2 + 3r_H^4))\theta^2}{r^2(R^2 - r_H^2)^2(R^2(r^4 + r_H^4) - r^2(R^4 + r_H^4))} + O(\theta)^4, \\
W(r, \theta) &= \frac{4\sqrt{2}R(R^2 - r_H^2)(R^2 + r_H^2)r^2r_H^2(r^2 + r_H^2)^2\sqrt{R^4 + r_H^4}}{r^4(R^2 - r_H^2)^2 + r_H^4(R^2 - r_H^2)^2 + r^2(6R^4r_H^2 + 4R^2r_H^4 + 6r_H^6)} + O(\theta)^2.
\end{aligned} \tag{B.7}$$

The expansion at  $\theta = \pi/2$  which holds for any values of  $r$  is

$$\begin{aligned}
f_0(r, \theta) &= \frac{r^4(R^2 - r_H^2)^2 + r_H^4(R^2 - r_H^2)^2 - 2r^2r_H^2(3R^4 + 2R^2r_H^2 + 4r_H^4)}{-\frac{32r^6(R^2 + r_H^2)^6(R^4 + r_H^4)}{(r^2 - r_H^2)^2} + \frac{(R^2 - r_H^2)^6(r^2 + r_H^2)^2(r^2R^2 + R^2r_H^4 + r^2(R^4 + r_H^4))}{r_H^4}} \\
&\quad \times \frac{r^4R^2(R^2 - r_H^2)^4(1 + \frac{r_H^4}{r^4} + \frac{R^4 + r_H^4}{r^2R^2})}{r_H^4} + O(\theta - \frac{\pi}{2})^2, \\
f_1(r, \theta) &= \frac{(r^2 + r_H^2)^4}{r^8(1 + \frac{r_H^4}{r^4} + \frac{R^4 + r_H^4}{r^2R^2})} + O(\theta - \frac{\pi}{2})^2, \\
f_2(r, \theta) &= \frac{R^2(r^2 + r_H^2)^4}{r^2(r^2 + R^2)(r^2R^2 + r_H^4)}(\theta - \frac{\pi}{2})^2 + O(\theta - \frac{\pi}{2})^4, \tag{B.8}
\end{aligned}$$

$$\begin{aligned}
f_3(r, \theta) &= \frac{1}{r^2R^2(R^2 - r_H^2)^4(r^2 + r_H^2)^2} \left( r^8R^2(R^2 - r_H^2)^4 + R^2r_H^8(R^2 - r_H^2)^4 + \right. \\
&\quad r^6(R^2 - r_H^2)^2(R^2 + r_H^2)^4 + r^2r_H^4(R^2 - r_H^2)^2(R^2 + r_H^2)^4 + r^4(6R^{12}r_H^2 + 26R^{10}r_H^4 \\
&\quad \left. + 66R^8r_H^6 + 60R^6r_H^8 + 26R^2r_H^{12} + 6r_H^{14}) \right) + O(\theta - \frac{\pi}{2})^2, \\
W(r, \theta) &= 4\sqrt{2}r^4Rr_H^2(R^2 - r_H^2)(R^2 + r_H^2)^3\sqrt{R^4 + r_H^4} \\
&\quad \times \left( r^8R^2(R^2 - r_H^2)^4 + R^2r_H^8(R^2 - r_H^2)^4 \right. \\
&\quad \left. + r^6(R^2 - r_H^2)^4 + r^2r_H^4(R^2 - r_H^2)^2(R^2 + r_H^2)^4 + r^4(6R^{12}r_H^2 + 26R^{10}r_H^4 \right. \\
&\quad \left. + 66R^8r_H^6 + 60R^6r_H^8 + 26R^2r_H^{12} + 6r_H^{14}) \right)^{-1} + O(\theta - \frac{\pi}{2})^2.
\end{aligned}$$

## References

- [1] S. W. Hawking and G. F. R. Ellis, Cambridge University Press, Cambridge, 1973
- [2] F. R. Tangherlini, Nuovo Cim. **27** (1963) 636.
- [3] R. C. Myers and M. J. Perry, Annals Phys. **172** (1986) 304.
- [4] R. Emparan and H. S. Reall, Phys. Rev. Lett. **88** (2002) 101101 [arXiv:hep-th/0110260].
- [5] R. Emparan and H. S. Reall, Phys. Rev. D **65** (2002) 084025 [arXiv:hep-th/0110258].
- [6] R. Emparan and H. S. Reall, Living Rev. Rel. **11** (2008) 6 [arXiv:0801.3471 [hep-th]].
- [7] K. Maeda, T. Shiromizu and T. Tanaka, eds., *Higher dimensional black holes*, Progress in Theoretical Physics Supplement, 189, (2011).
- [8] G. T. Horowitz, ed., *Black Holes in Higher Dimensions*, (Cambridge University Press, Cambridge, 2012).
- [9] H. S. Reall, Int. J. Mod. Phys. D **21** (2012) 1230001 [arXiv:1210.1402 [gr-qc]].

- [10] R. Emparan, T. Harmark, V. Niarchos, N. A. Obers and M. J. Rodriguez, JHEP **0710** (2007) 110 [arXiv:0708.2181 [hep-th]].
- [11] R. Emparan, T. Harmark, V. Niarchos and N. A. Obers, Phys. Rev. Lett. **102** (2009) 191301 [arXiv:0902.0427 [hep-th]].
- [12] R. Emparan, T. Harmark, V. Niarchos and N. A. Obers, JHEP **1003** (2010) 063 [arXiv:0910.1601 [hep-th]].
- [13] R. Emparan, T. Harmark, V. Niarchos and N. A. Obers, JHEP **1004**, 046 (2010) [arXiv:0912.2352 [hep-th]].
- [14] B. Carter, arXiv:1112.2094 [hep-th].
- [15] H. Kudoh, Phys. Rev. D **75** (2007) 064006 [arXiv:gr-qc/0611136].
- [16] B. Kleihaus, J. Kunz and E. Radu, Phys. Lett. B **678** (2009) 301 [arXiv:0904.2723 [hep-th]].
- [17] B. Kleihaus, J. Kunz, E. Radu and M. J. Rodriguez, JHEP **1102** (2011) 058 [arXiv:1010.2898 [gr-qc]].
- [18] B. Kleihaus, J. Kunz and E. Radu, Phys. Lett. B **718** (2013) 1073 [arXiv:1205.5437 [hep-th]].
- [19] B. Kleihaus, J. Kunz and E. Radu, Phys. Lett. B **723** (2013) 182 [arXiv:1303.2190 [gr-qc]].
- [20] Ó. J. C. Dias, J. E. Santos and B. Way, JHEP **1407** (2014) 045 [arXiv:1402.6345 [hep-th]].
- [21] O. J. C. Dias, P. Figueras, R. Monteiro, J. E. Santos and R. Emparan, Phys. Rev. D **80** (2009) 111701 [arXiv:0907.2248 [hep-th]].
- [22] O. J. C. Dias, P. Figueras, R. Monteiro and J. E. Santos, Phys. Rev. D **82**, 104025 (2010) [arXiv:1006.1904 [hep-th]].
- [23] H. Kudoh and T. Wiseman, Prog. Theor. Phys. **111** (2004) 475 [hep-th/0310104].
- [24] T. Harmark and N. A. Obers, JHEP **0205** (2002) 032 [hep-th/0204047].
- [25] R. Emparan and H. S. Reall, Class. Quant. Grav. **23** (2006) R169 [hep-th/0608012].
- [26] B. Kleihaus, J. Kunz and E. Radu, JHEP **1002** (2010) 092 [arXiv:0912.1725 [gr-qc]].
- [27] S. Stotyn, C. D. Leonard, M. Oltean, L. J. Henderson and R. B. Mann, Phys. Rev. D **89** (2014) 044017 [arXiv:1307.8159 [hep-th]].
- [28] J. Kunz, F. Navarro-Lerida and J. Viebahn, Phys. Lett. B **639** (2006) 362 [hep-th/0605075].
- [29] J. Kunz and F. Navarro-Lerida, Phys. Lett. B **643** (2006) 55 [hep-th/0610036].
- [30] Y. Brihaye, B. Kleihaus, J. Kunz and E. Radu, JHEP **1011** (2010) 098 [arXiv:1010.0860 [hep-th]].
- [31] M. Allahverdizadeh, J. Kunz and F. Navarro-Lerida, Phys. Rev. D **82** (2010) 024030 [arXiv:1004.5050 [gr-qc]].
- [32] M. Allahverdizadeh, J. Kunz and F. Navarro-Lerida, Phys. Rev. D **82** (2010) 064034 [arXiv:1007.4250 [gr-qc]].
- [33] W. Schönauer and R. Weiß, J. Comput. Appl. Math. **27**, 279 (1989) 279;  
M. Schauder, R. Weiß and W. Schönauer, The CADSOL Program Package, Universität Karlsruhe, Interner Bericht Nr. 46/92 (1992).

- [34] J. M. Bardeen and G. T. Horowitz, Phys. Rev. D **60** (1999) 104030 [hep-th/9905099].
- [35] H. Elvang, R. Emparan and A. Virmani, JHEP **0612**, 074 (2006) [hep-th/0608076].
- [36] M. Headrick, S. Kitchen and T. Wiseman, Class. Quant. Grav. **27** (2010) 035002 [arXiv:0905.1822 [gr-qc]].
- [37] C. Herdeiro, B. Kleihaus, J. Kunz and E. Radu, Phys. Rev. D **81** (2010) 064013 [arXiv:0912.3386 [gr-qc]];
- [38] C. Herdeiro, E. Radu and C. Rebelo, Phys. Rev. D **81** (2010) 104031 [arXiv:1004.3959 [gr-qc]].
- [39] J. Armas and T. Harmark, arXiv:1402.6330 [hep-th].
- [40] B. Kleihaus, J. Kunz and K. Schnülle, Phys. Lett. B **699** (2011) 192 [arXiv:1012.5044 [hep-th]].
- [41] M. M. Caldarelli, R. Emparan and M. J. Rodriguez, JHEP **0811** (2008) 011 [arXiv:0806.1954 [hep-th]].
- [42] J. Armas and N. A. Obers, Phys. Rev. D **83** (2011) 084039 [arXiv:1012.5081 [hep-th]].
- [43] R. Emparan and P. Figueras, JHEP **1011** (2010) 022 [arXiv:1008.3243 [hep-th]].
- [44] A. A. Pomeransky and R. A. Sen'kov, arXiv:hep-th/0612005.
- [45] O. J. C. Dias, G. T. Horowitz and J. E. Santos, JHEP **1107** (2011) 115 [arXiv:1105.4167 [hep-th]].